Modeling the outer rings of SN 1987A

Erik B. Johansson

20000308 4:20 PM

1 Abstract

A model suggested by Soker (1999) for the formation of the rings of SN 1987A has been investigated in numerical hydrodynamical simulations. The main new ingredient in this model is a short pulse of mass ejection caused by a merger with a companion star, a few thousand years before the RSG contracts into a BSG, which results in a hollowed torus with the cross-section of a horse shoe. The BSG wind sweeps up the dense end-points of the horse shoe to form the outer rings of SN 1987A. Simulations show that the model can produce two rings with properties similar to the outer rings of SN 1987A, although they end up within the inner ring. The result is thus one outer ring, and two inner rings. The implementation of the intermediate wind is critical and the model needs a more physical description of this phase. Also, the present theory of SN 1987A relies mainly on ionization effects, which is not included in the model and needs to be investigated.

Contents

1 Abstract **i**

2 Introduction **1**
2.1 History . . . 1
2.2 Earlier models . . . 2
2.2.1 Interacting winds . . . 2
2.2.2 Ionization . . . 3
2.2.3 Beamed jets . . . 4
2.2.4 Other models . . . 4
2.3 New model . . . 4

3 Numerical method and equations **6**
3.1 Theory . . . 6
3.2 The time step . . . 9
3.3 Boundary conditions . . . 9
3.4 Initial conditions . . . 10
3.5 Short cuts . . . 11
3.6 Constraints on the model . . . 12

4 Results **13**
4.1 The intermediate wind . . . 13
4.2 The red wind . . . 18
4.3 The blue wind . . . 27

5 Conclusions **38**

6 Acknowledgements **38**

A Appendix:Description of the interface program **40**
A.1 Introduction . . . 40
A.2 Menu buttons . . . 40
A.2.1 Start . . . 40
A.2.2 Quit . . . 40
A.2.3 Draw . . . 40
A.2.4 Set . . . 41
A.3 Running a simulation . . . 43
A.4 File format . . . 44

2 Introduction

2.1 History

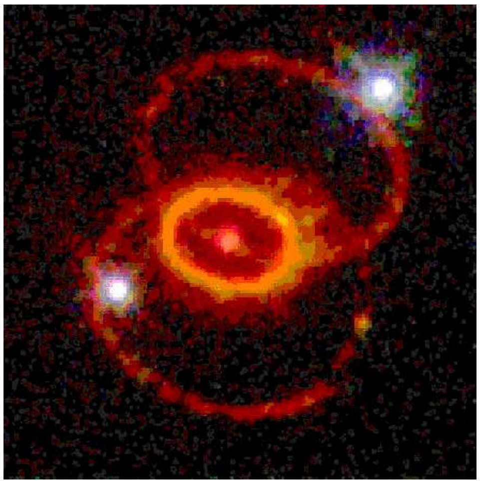

Figure 1: SN 1987A

A hundred and seventy thousand years ago, the Large Magellanic Clouds shook, when the blue super giant Sanduleak -69° 202 collapsed and exploded.

Intergalactic news travels slowly.

At 9:30, 24 February 1987, Ian Shelton detected supernova 1987A using a 10 inch astrograph at Las Campanas Observatory in Chile. This was the first time since the 17:th century that an observable supernova occurred so close to us, and astronomers all over the world leaped with joy at this unique chance to study a supernova close up. A supernova occurs every thirty years or so in our own galaxy but, as most of our galaxy is invisible to us, observable supernovae are rare. SN 1987A seemed to behave odd until it was realized that the progenitor was a blue super giant, as opposed to a red super giant which is usually the case. Since the discovery, SN 1987A has been studied by an army of astronomers, who rejoiced when many of their theories of supernovae where confirmed.

One of the mysteries that remains unsolved, and the subject of this thesis, is the origin of the rings around SN 1987A. There is a pair of two large, thin rings, and a broader, much denser, inner ring (see fig.1) The first Hubble Space Telescope (HST) pictures showed the outer rings as two arcs, that became two closed rings a few years after. This was because the light of the supernova explosion had not reached the whole structure, thus only parts of the rings where illuminated. (An important conclusion from this is that the rings were not ionized at the time of the supernova explosion - unionized matter is dark).

The outer rings have some peculiar properties.

1. They are not identical. The northern ring has a semi-major axis of 1.77", and a semi-minor axis of 1.30" while the southern ring has a semi-major axis of 1.84" and a semi-minor axis of 1.58".

2. A line drawn from the centre of the northern ring to the centre of the southern ring is displaced from the central star by 0.4". This corresponds to a displacement of $\sim 10\%$ to the size of the rings.

3. The outer rings are a 100 times denser than their surroundings.

4. The nitrogen abundances are much lower in the outer rings than in the inner ring (Panagia et al. 1996). This indicates that the outer rings are made of much earlier ejecta, before the progenitor has had much time to mix up heavy elements from the core.

5. From observations it is also found that the inner ring has a sharp inner edge. The outer edge is blurred, giving an impression that the ring is connected to the outer rings with a cone-like wall.

Since the supernova occurred there have been numerous attempts to explain the the mechanism forming the outer rings, and no completely satisfactory model has yet been reached.

2.2 Earlier models

A big problem, or a great relief, for astronomers trying to model SN 1987A is that even though the resolution of the HST is very high, SN 1987A is poorly resolved. The ground based observations of the Hourglass nebula, which is planetary nebula "only" 8000 ly away, showed a similar double ring structure which turned out to be a whole collection of rings when one had a look at it with the HST. Because of this problem there are almost as many different scenarios and models suggested as there are papers published on the subject.

2.2.1 Interacting winds

The interacting winds model can be said to be the standard model for the formation of the rings around SN1987A. One assumes that the progenitor, in its red super giant (RSG) phase, had an asymmetric mass loss concentrated in the equatorial plane, e.g due to rotation or tidal pull from a binary companion. The following high velocity blue super giant (BSG) wind forms

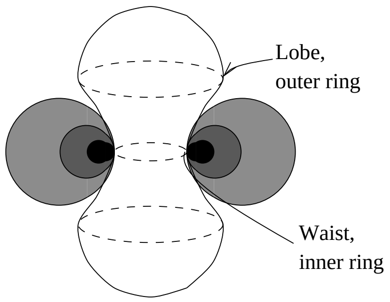

Figure 2: Formation of an hourglass shell

a two lobed bubble with walls of shocked RSG wind as its expansion is blocked by the asymmetric density distribution from the previous wind, see fig.2. The inner ring forms when the slowly expanding equatorial RSG wind is swept up by the fast wind. The outer rings where thought to be a limb brightening effect of the lobes when the shell was lit up by the strong UV-radiation following the SN explosion. The first 2D simulations where done by Blondin & Lundqvist in 1993 and the parameter values they derived have become a standard set which are used or referred to in all following interactive wind models.
There are some problems with this model. The observed expansion velocities of the inner and outer rings are much lower than those from simulations. Also, the outer rings are too sharp and narrow to be projections of a shell with almost spherical curvature. No shell has been observed around SN 1987A, hence the standard model can not explain the outer rings.
This model has been developed further in different ways. Lloyd, O'Brien & Kahn (1995) investigated the effect of a binary companion interacting with the RSG wind of the progenitor. The result is a double-cone like structure, which at the onset of the BSG wind is swept up into two rings forming the outer rings of SN 1987A.

2.2.2 Ionization

Recently the winds have changed, so to speak, for the models of the pre-flash SN evolution. Chevalier & Dwarkadas (1995) made a model where the BSG ionizes the surrounding RSG wind, rather than producing a wind which pushes it. The evidence supporting this is the X-ray and radio emission which has been detected. The BSG ionizes a region increasing in radii with the ionization velocity which is super sonic. As the region grows, and density drops, the ionization velocity drops below the sound speed and a shock front is formed at the intersection of the high pressure HII-region and the outside HI region. Assuming asymmetry for the RSG wind, this gives a similar hour-glass structure as for the interacting winds model. The model sets an upper limit on the mass loss rate from the BSG which is much lower than in the standard model.

Meyer (1997) further investigated the effect of an asphericity in the density distribution for the RSG wind. He found that it leads to high density peaks forming at the steepest point in the distribution gradient. These then cool to become the outer rings of SN 1987A, and are not ionized at the time of the supernova.

2.2.3 Beamed jets

Burdeli & King (1995) suggest that a pulsar is formed after the supernova, resulting in two collimated precessing jets of relativistic particles from the poles. The star has already gone through its red and blue phase, forming the hourglass shape. The jets hit the lobes of the hourglass, and as the pulsar rotates it draws two thin circles compressing matter into two very sharp rings.

2.2.4 Other models

Many other models have been suggested, e.g one by Washimi et. al (1996) who claim that magnetic mechanisms form the rings. Other people have tried to apply, or combine, the theory for the formation of planetary nebulae (PNe) on SN 1987A with varying results.

2.3 New model

Many have argued for a binary companion of Sanduleak -69° 202, the progenitor of SN 1987A, mainly because a binary would explain the aspherical RSG wind which is needed to form the inner ring. There are some other indications for a binary companion, e.g the high metallicity of the circumstellar gas around SN 1987A. A merger or close interaction with a binary could help mix up heavy elements from the core of the star to the envelope. Binaries are not rare, at least half of the stars we can see are parts of binary systems.

Noam Soker (*A model for the outer rings of SN 1987A*, 1999) suggested a model where a third ingredient of the uncertain final stages of the dying star is added to the standard interacting winds model. Here is a short summary of the model:

The idea is that a few thousand years before the RSG contracts into a BSG, a binary companion enters the envelope of the progenitor. The result is a short pulse of very dense high velocity wind that is concentrated in the equatorial region. The transfer of momenta spins up the progenitor, giving it a much more asymmetric mass loss. The merger may also be the reason for the RSG turning into a BSG, a few thousand years later. In order to avoid the potential confusion brought on by the number of different winds and mass-losses, it is wise to follow Sokers example and divide the problem into four phases, see also fig.3.

Phase 1. Slow, dense wind from the RSG. The mass-loss might be slightly higher in the equatorial region due to rotation or tidal interaction with a binary companion. This phase has lasted for many thousand years, thus the whole area around the RSG is filled with an asymmetric distribution of the slow, dense wind.

Phase 2. The binary companion enters the envelope of the RSG progenitor. A short pulse, a few $\times$ 10 years, of ejecta from the merger results in a wind with higher velocity and density, concentrated in the equatorial plane. As this intermediate wind runs into the slow wind, a high pressure region is formed. The pressure forces the region to expand into a shell, and as there is no slow-wind material inwards, the shell gets the cross-section of a horse-shoe. The end-points of the horse-shoe, i.e the region nearest the progenitor, gets a higher density and lower velocity than the rest of the structure.

Phase 3. The RSG wind resumes, now much more concentrated in the equatorial direction due to the fast rotation of the progenitor. Meanwhile the horse-shoe torus is expanding, and is being elongated in the equatorial direction further increasing the density contrast of the end-points.

Phase 4. A few thousand years after the merger, the progenitor shrinks to a BSG and blows a fast, thin wind. The contraction of the rotating RSG spins up the envelope of the progenitor which may give it higher mass loss in the equatorial region. The wind pushes the surrounding material outwards to large distances. The dense regions around the equator from the third phase and the horse-shoe end-points are accelerated less and thus left behind. These grow to form the inner and outer rings of SN 1987A.

This model would account for

1. The slow motion of the outer rings. [1]
2. The high density contrast of the outer rings.

[1] Until very recently it was believed that the outer rings must have a low velocity to make up for them being so close to the inner rings. If they are created by much earlier ejecta, one argued, they must have been traveling for a much longer time. Crotts & Heathcote (2000) published measurements of the outer rings where the velocity ratio for the inner and outer rings is equal to the radius ratio, 26 km/s vs. 23 km/s for the outer rings and 10.5 km/s for the inner ring. The rings were thus all created at the same time, but this was unknown to Soker (1999).

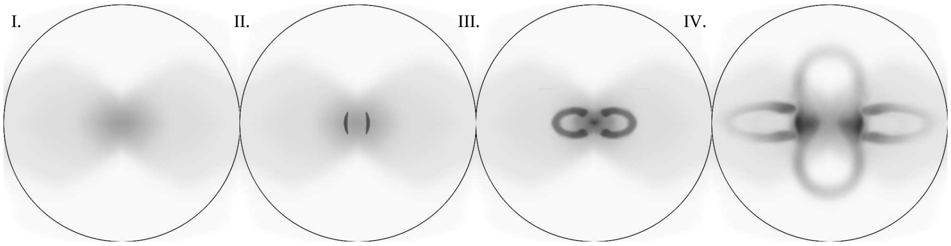

Figure 3: A sketch of the four phases

3. The displacement of the outer rings, if the binary was in an eccentric orbit. Also, the time-scale of the intermediate wind, being of an order of a few orbital periods, is short enough to let small perturbations give large scale results.

3 Numerical method and equations

3.1 Theory

The state of a fluid can be described by the variables ρ - the density, v - the velocity and p - the pressure. The equations for the conservation of mass, momentum and energy are the Euler equations:

$$\begin{cases} \frac{\partial \rho}{\partial t} + \nabla \cdot \rho \mathbf{v} & = 0 \quad \text{(conservation of mass)} \\ \frac{\partial \rho \mathbf{v}}{\partial t} + \nabla \cdot \rho \mathbf{v} \cdot \mathbf{v} + \nabla p & = \mathbf{f} \quad \text{(conservation of momentum)} \\ \frac{\partial e}{\partial t} + \nabla \cdot (e+p)\mathbf{v} & = s_e \quad \text{(conservation of energy)} \end{cases} \tag{3.1}$$

where we assume no external forces, energy terms or viscosity, $\mathbf{f} = s_e = 0$. For economic reasons we assume cylindrical symmetry and can thus limit our description to two dimensions. Following Mellema et al. (1989) we use spherical polar coordinates, and can thus rewrite the Euler-equations as

$$\frac{\partial \mathbf{W}}{\partial t} + \frac{\partial \mathbf{F}}{\partial r} + \frac{\partial \mathbf{G}}{\partial \theta} = \mathbf{S} \tag{3.2}$$

where $\mathbf{W}$ is the *state vector*, $\mathbf{F}$ and $\mathbf{G}$ are the *flux vectors* in the radial and angular direction, and $\mathbf{S}$ is the *source vector*.

$$\begin{aligned} \mathbf{W} &= r^2 \sin\theta(\rho, \rho v_r, \rho v_\theta, e) \\ \mathbf{F} &= r^2 \sin\theta(\rho v_r, \rho v_r^2 + p, \rho v_r v_\theta, (e+p)v_r) \\ \mathbf{G} &= r^2 \sin\theta(\rho v_\theta, \rho v_r v_\theta, \rho v_\theta^2 + p/r^2, (e+p)v_\theta) \\ \mathbf{S} &= r^2 \sin\theta(0, 2p/r + r\rho v_\theta^2, \tfrac{p\cos\theta}{r^2 \sin\theta}, 0) \end{aligned} \tag{3.3}$$

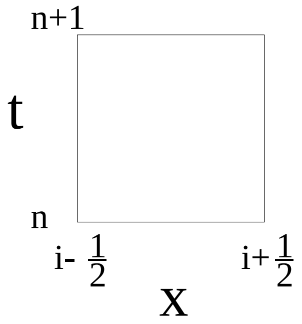

Figure 4: Single grid cell

The total energy e is the sum of the internal and kinetic energy,

$$\begin{aligned} e_{tot} &= e_{int} + e_{kin} \\ e_{kin} &= \tfrac{1}{2}\rho(v_r^2 + r^2 v_\theta^2) \\ e_{int} &= \tfrac{p}{\gamma-1} = \tfrac{\rho k T}{\mu m_H(\gamma-1)} \text{ (Assuming an ideal gas)} \end{aligned} \tag{3.4}$$

To the dismay of theoreticians this is a field in physics where numerical methods are necessary. The method applied must be able to treat discontinuities (shocks) well, and also keep the quantities conserved.

One begins with defining a grid of $n \times m$ cells, where each cell contains the state values of a finite volume $dV = dr d\theta$ at time $t = t_0 + n\Delta t$. Because there are no well established methods to solve these equations in two dimensions, some way of reducing the problem to one dimension is necessary. The technique used here is called *operator splitting*; it is possible to show that one can solve

$$\frac{\partial \mathbf{W}}{\partial t} + \frac{\partial \mathbf{F}}{\partial r} + \frac{\partial \mathbf{G}}{\partial \theta} = \mathbf{S} \tag{3.5}$$

to second order accuracy by for each time step first integrating

$$\frac{\partial \mathbf{W}}{\partial t} + \frac{\partial \mathbf{F}}{\partial x} = \mathbf{R} \tag{3.6}$$

over half a time step. With the new state obtained integrating

$$\frac{\partial \mathbf{W}}{\partial t} + \frac{\partial \mathbf{G}}{\partial \theta} = \mathbf{T} \tag{3.7}$$

over a full time step, and then eqn. 3.6 over half a time step again. $\mathbf{R}+\mathbf{T} = \mathbf{S}$ can in principle be chosen arbitrarily. Now looking at the problem in one dimension, the differential equation

$$\frac{\partial \mathbf{W}}{\partial t} + \frac{\partial \mathbf{F}}{\partial x} = \mathbf{S} \tag{3.8}$$

can by Gauss' theorem be integrated around a closed contour C (defined in $\{x,t\}$-space) to give the integral expression

$$\oint_C (\mathbf{W}dx + \mathbf{F}dt) = \oint_C \mathbf{S}dxdt \tag{3.9}$$

We set up a one dimensional grid of cells given by $x_i = x_0 + i\Delta x$, at $t = t_0 + n\Delta t$ (see fig.4), using a row or column from the two dimensional grid and make the approximation that the state of a cell is stationary and constant within the cell boundaries. With eqn. 3.9 one solves for $\mathbf{W}$

$$\langle \mathbf{W}_i \rangle^{n+1} = \langle \mathbf{W}_i \rangle^n + \frac{\Delta t}{\Delta x}(\mathbf{F}^{n+1/2}_{i-1/2} - \mathbf{F}^{n+1/2}_{i+1/2}) + \mathbf{S}^{n+1/2}_i \Delta t \tag{3.10}$$

where $\langle \mathbf{W} \rangle$ is the mean state value. What remains to be done is finding a way to calculate the interface fluxes at $n+1/2$ from the mean state values at n. We have chosen to use an approximate *Riemann Solver*, or a *Roe Solver* (Roe 1982, also Eulderink & Mellema 1995). To keep it short the method is briefly described with the following steps:

1. Calculate $\mathbf{F}^n_i$ – the flux at the cell centre at n, from $\langle \mathbf{W}_i \rangle^n$, the mean state values of the cell at the same position in {x,t} phase space.

2. Calculate the flux at the interfaces and the flux difference

$$\begin{aligned} \mathbf{F}^n_{i-1/2} &= \mathbf{F}^n_{i-1} + \frac{1}{2}\mathbf{S}^n_{i-1}\Delta x \\ \mathbf{F}^n_{i+1/2} &= \mathbf{F}^n_i - \frac{1}{2}\mathbf{S}^n_i \Delta x \\ \mathbf{\Delta}^n_i &= \mathbf{F}^n_{i+1/2} - \mathbf{F}^n_{i-1/2} \end{aligned}$$

3. Approximate $\mathbf{F}$ as a (locally) linear function of $\mathbf{W}$, $\mathbf{F} = \widetilde{\mathbf{A}}\mathbf{W}$. Calculate the eigenvalues and eigenvectors of the locally constant matrix $\widetilde{\mathbf{A}}$.

4. Calculate the projection of the flux difference $\mathbf{\Delta}^n_i$ across the interface.

5. Finally calculate $\mathbf{F}^{n+1/2}_{i+1/2}$ with

$$\mathbf{F}^{n+1/2}_{i+1/2} = \frac{1}{2}(\mathbf{F^n_i} + \mathbf{F^n_{i+1/2}}) - \frac{1}{2}\sum_k \sigma_k a_k \mathbf{e_k} \tag{3.11}$$

where

$$\sum_k a_k \mathbf{e_k} = \mathbf{\Delta}^n_i \tag{3.12}$$

$$\sigma_k = sign(\lambda_{\mathbf{k}} \frac{\Delta t}{\Delta x}) \tag{3.13}$$

(Step interpolation, gives first order approximation)

$$\sigma_k = \lambda_{\mathbf{k}} \frac{\Delta t}{\Delta x} \tag{3.14}$$

(Linear interpolation, gives second order approximation)

A problem with the second order scheme is that it will produce some ripples at discontinuities. Linear interpolation will make the Roe solver conserve, and encourage, sharp discontinuities while step interpolation tends to smooth them out. In order to balance the two, a function, *super-B*, is used which uses the first order coefficients at discontinuities, and the second order otherwise. A parameter determines how strong the discontinuity needs to be to make *super-B* use first order coefficients. Roe recommends a value for this parameter of 2.0, but it may be lowered at troublesome phases in the simulation.

3.2 The time step

The speed with which information travel is the sum of the local velocity and the local speed of sound. One must therefore adjust the time step to ensure that information cannot travel further than the nearest cell. The ratio $\frac{\Delta x}{(v+s)}$ is calculated for every cell, where v is the local velocity and s is the local sound speed. The radial length of the cell is Δr and its azimuthal height is $r\Delta\theta$, so Δx is simply the minimum of these two. The smallest ratio available on the grid is chosen, and is for safety multiplied by $\frac{1}{2}$ to give a time step which works for all cells.[2]

3.3 Boundary conditions

Two grid cells along the border of the total grid are reserved for boundary values. Assuming cylindrical symmetry one only needs to model one quarter of the plane, from equator to pole, and let the boundary cells at the axes be reflection boundaries. This means that the values of a cell at the axis is copied to a cell at the opposite side of the axis, but with mirrored velocity (see fig.5).

To obtain an outer boundary over which the wind shall float when leaving the grid, the two last columns of cells are given the values of the last “proper” column.

The first cells are where the winds make their first appearance. The choice of which values to put in these cells is important, as this kind of

[2]The $\frac{1}{2}$ term is also necessary to give the *operator splitting* approximation second order accuracy.

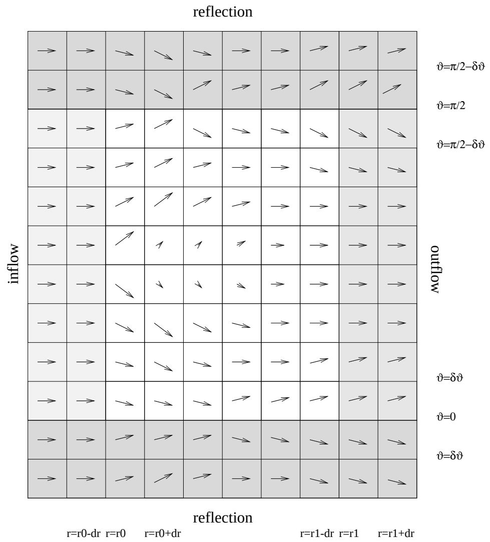

Figure 5: Grid with boundary cells

hydro-code is quite unstable. First one calculates the density using the mass loss and wind velocity of the star, with the radius of the first grid cell. Using the temperature of the wind, along with the density and velocity, one can calculate the momentum and energy. These values can be used in three ways:

1. The most natural choice is to use a *velocity driven* wind, i.e we simply put in the the density, momentum and energy unaltered.

2. One might assume that the gas is shocked even before entering the grid, in which case a condition of a stationary shock is to be used.

3. One could also give the wind zero velocity, and let it's thermal energy build up a pressure front which engine the flow of material onto the grid; a *pressure driven* wind.

In the simulations method 1 was used for the slower winds and method 2 for the fast blue super giant wind.

3.4 Initial conditions

The grid is initially filled with slow RSG wind, using the parameters dM, v_r, v_θ and T. Assuming the velocity is radial, $v = v_r$, the density is given by

$$\rho(r) = \frac{\dot{M}}{4\pi v r^2} \tag{3.1}$$

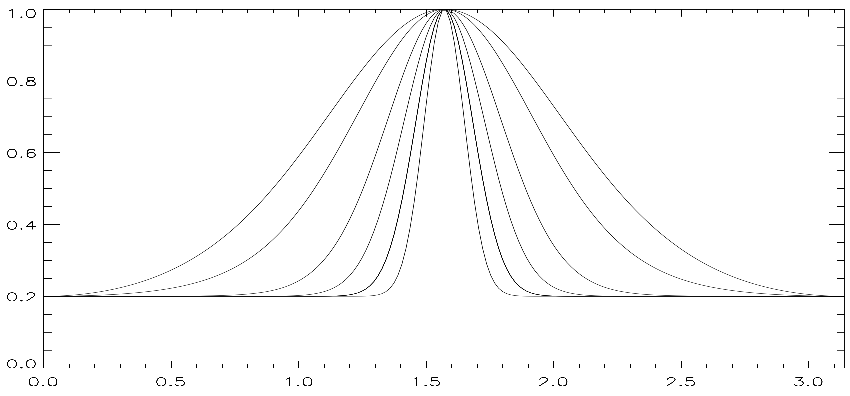

Figure 6: The distribution function $f(\theta)$ plotted for $Q = 5$, $\beta = 1,2,5,10,20$

In order to create the asymmetry of density one needs a distribution function $f(\theta)$. The function chosen is one which was suggested by Blondin & Lundqvist (1993), referred to as the inverse Icke function:

$$f(\theta) = 1 - \alpha\Big(\frac{\exp(-2\beta\cos^2\theta) - 1}{\exp(-2\beta) - 1}\Big) \tag{3.2}$$

with the exception that it is not normalized to give a total value of 1 when integrated over θ. The parameters α and β determine the shape of the function. α is calculated as

$$\alpha = 1 - \frac{1}{Q} \tag{3.3}$$

where Q is the ratio between the mass loss in the equatorial and polar direction,

$$Q = \frac{dM_{equator}}{dM_{pole}} \tag{3.4}$$

β is a steepness parameter, $\beta = 1$ gives a smooth transition from pole to equator where $\beta \gg 1$ gives a distribution strongly peaked at the equator. f is plotted in fig.6 for different values of β.

The asymmetrical density distribution is then given by

$$\rho(r, \theta) = f(\theta)\rho(r) \tag{3.5}$$

3.5 Short cuts

As mentioned above, the code is unstable and is likely to produce unwanted effects. The problem areas are generally the axes, where in-falling matter encounters it's own mirrored image and therefore reflects in a rather unphysical way. Also, the second order scheme of the Roe solver induces oscillations which can lead to negative pressures. The nicest solution is to lower the *super-bee* parameter, as mentioned in section 3.1.

Unfortunately this is not always enough. Negative pressures pop up, which in turn can lead to negative densities. One therefore has to deal with these in some clever way.

The Roe-solver code itself checks the calculated fluxes to see if they will lead to a negative pressure or density. If so, it uses the first order projection coefficients for the particular cell. After the whole grid is updated, a new check will be made. If a cell still has a negative pressure, the energy of the cell is recalculated to give the same pressure as the lowest pressure of the four neighbouring cells.

Nothing can/should be done when a negative density turns up, because of the extreme unphysical nature of the problem. However one can prevent it from happening by smoothing the grid. Over all cells, the new state of a cell is given by

$$\mathbf{W}^*_{i,j} = \mathbf{W}_{i,j} + \epsilon(\mathbf{W}_{i-1,j} + \mathbf{W}_{i+1,j} + \mathbf{W}_{i,j-1} + \mathbf{W}_{i,j+1} - 4 \times \mathbf{W}_{i,j}) \quad (3.6)$$

The smoothing is done only when other measures like lowering the time step or super bee parameters are not enough. The amount of smoothing is determined by ϵ, a typical value of 1×10^{-5} has been used. Though ugly, the smoothing function at least conserves quantities - what disappears from one cell is inserted into its neighbour.

3.6 Constraints on the model

Each phase has its own set of parameter values, ρ, v, T, Q and β. With four phases this generates a ludicrous amount of possible combinations, and this thesis has to be constrained to show the basic workings of the model rather than trying to give a well calibrated solution.

As the highest velocities normally are found closest to the star, a small inner radius lowers the time step (see section 3.2). A reasonable value for the inner radius is $r_0 = 2 \times 10^{14}$m, which has been used in all simulations henceforth. In section 4.2 the choice of inner radius is further discussed.

Because the scale of the structure created during phase II is relatively small, $\sim 3 \times 10^{14}$m (see below), the outer radius must be chosen so that it is resolved with the grid resolution. Increasing the grid resolution gives drastically longer run-times for the simulations. At least 30 gridcells are needed to adequately resolve the second phase, which gives a maximal outer radius of $r_1 = 4 \times 10^{15}$m using a grid of 300×300 cells.

4 Results

As simulations are very time consuming it is important to investigate the parameters for each phase using low resolution before running the final, large scale simulations. The primary goal for this thesis has been set to investigate the formation of the horse-shoe structure described by Soker, as the amount of parameters make a deeper study of the final phases impossible. This section has been divided into four parts:

In section 4.1 we discuss and investigate the implementation of the intermediate wind, i.e phase II.

In section 4.2 we look into the evolution of the structure created during phase II, as the progenitor resumes its slow red wind in phase III.

In section 4.3 the effect of the blue wind is tested on the most interesting structures obtained during phase III. The evolution of the two best simulations are shown.

4.1 The intermediate wind

The crucial part of the idea behind this model is the intermediate wind which follows after the merger of the two stars. The first simulations of this were made by Soker (1989) using a technique called particle-in-cell. Due to the limited speed of computers in those days the simulations had a quite low resolution, 100×50 cells. It is therefore important to study this phase more carefully.

Soker propose a wind that lasts for about 50 years, with a total mass loss of $10^{-3} - 3 \times 10^{-2}$ $M_\odot$ and a velocity of 100 km/s. As the understanding of star-mergers is far from complete, an ad hoc approach has to be taken when implementing this wind.

In his simulations, Soker used a distribution function for the mass loss defined as

$$f_{Soker}(\theta) = \begin{cases} 0.04 - \cos^2\theta & \cos\theta \leq 0.2 \\ 0 & \cos\theta > 0.2 \end{cases} \tag{4.7}$$

and kept the velocity of the wind constant over θ. This gives a wind that is cut off at an angle roughly 10° from the equatorial axis, thus the cells above 10° are given an outflow condition. This scheme has advantages as well as draw backs. It seems unlikely that *no* matter is ejected above the 10°, which also implies that the RSG wind is turned off during the pulse. However, this somewhat crude method has properties that might be necessary for the model to work as will be discussed below.

We wanted to use a continuous function for the mass loss and velocity without making any extra flow structures. If there is mass loss in all directions, with a velocity higher than the surrounding RSG wind, it will drive a shock into the RSG wind, forming a closed shell around the star. This shell does not appear with Sokers scheme as there simply is no input above 10°

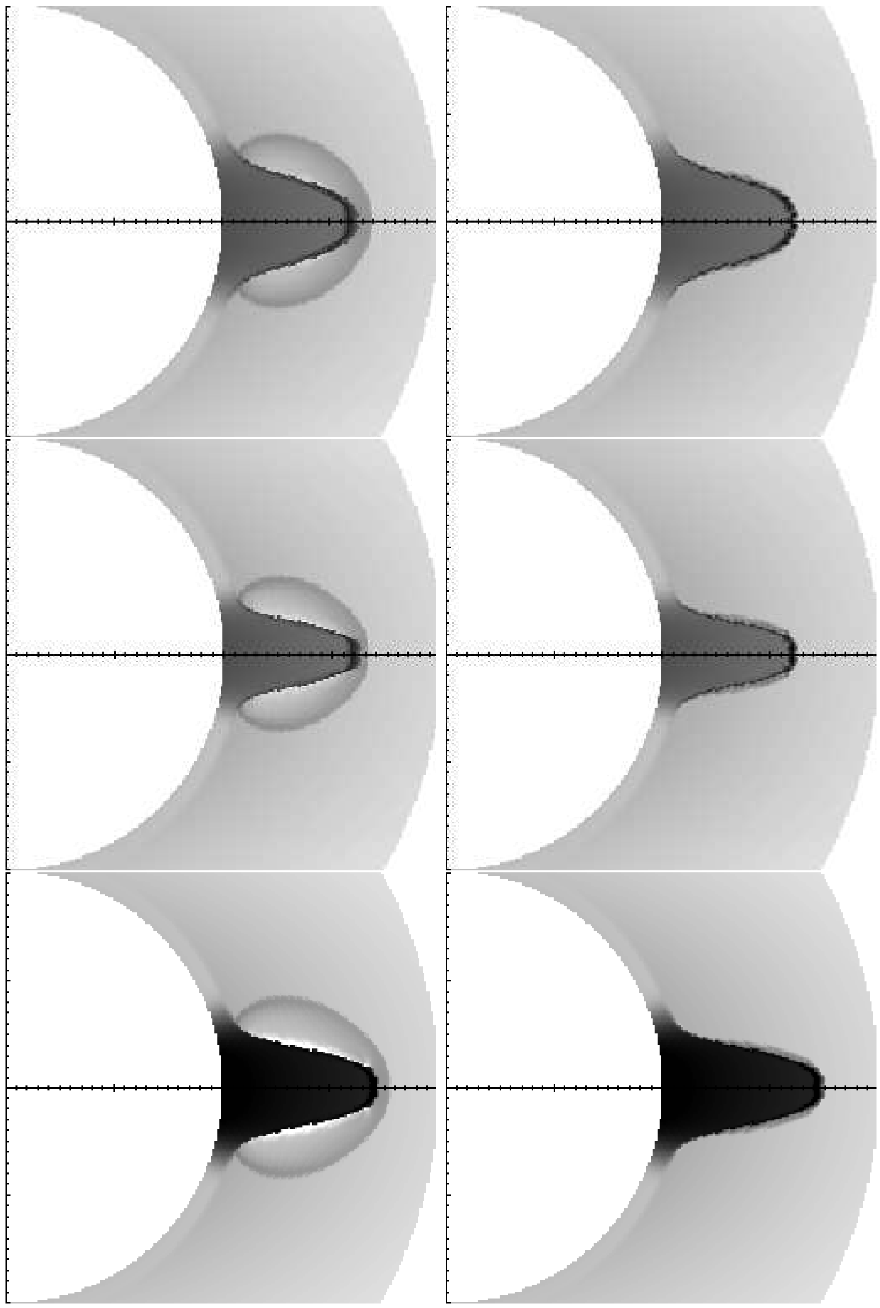

Figure 7: *The intermediate wind.* Logarithmic density plot of **interAA**(top), **interAB**(middle), **interAC**(bottom) after 50 years, scaling from $n = 6 \times 10^6$ cm^{-3} (black) to $n = 6$ cm^{-3} (white), $r_0 = 2 \times 10^{14}$m, $r_1 = 4 \times 10^{14}$m, $\gamma = 5/3$ (left) $\gamma = 1.05$ (right).

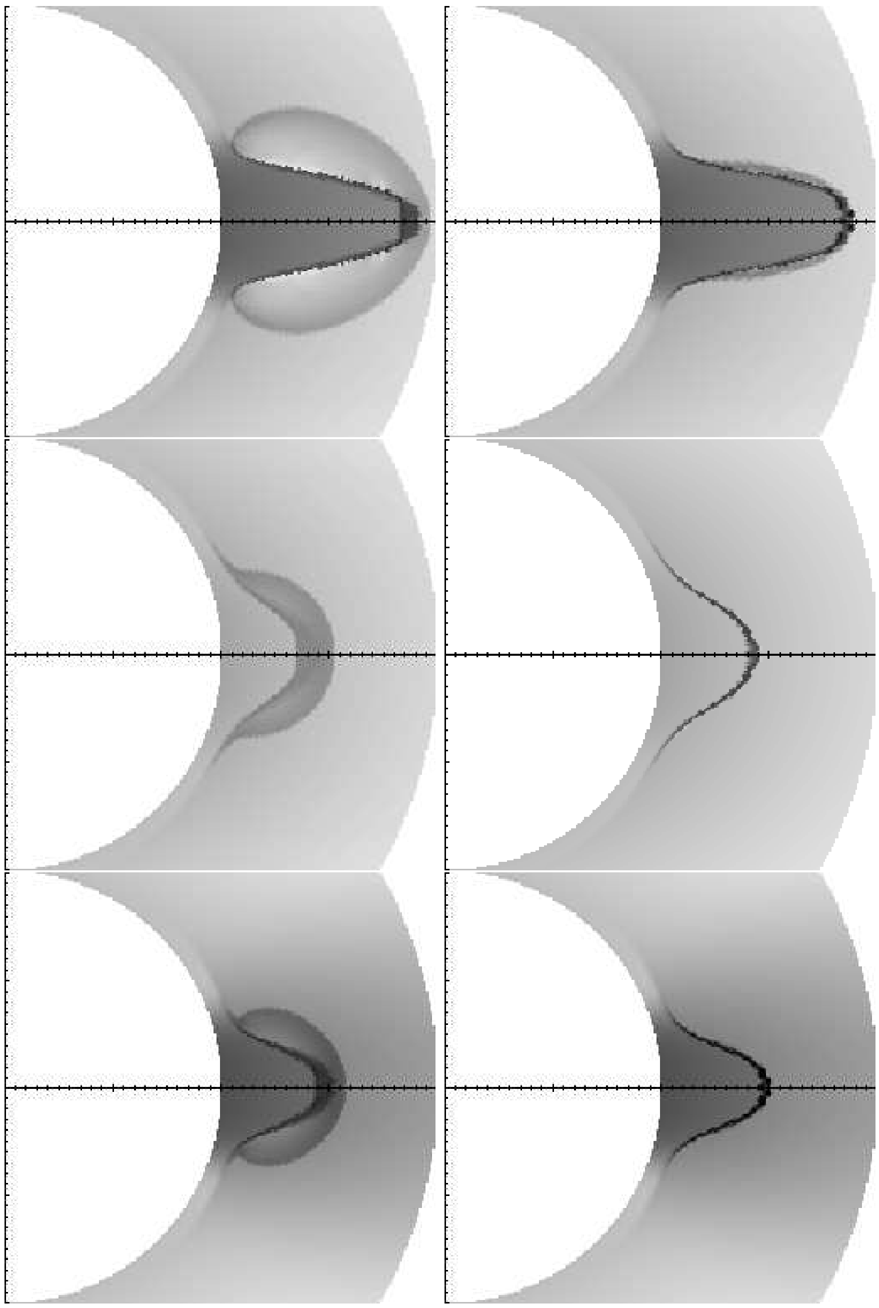

Figure 8: *The intermediate wind.* Logarithmic density plot of **interAD**(top), **interAE**(middle), **interBA**(bottom) after 50 years, scaling from $n = 6 \times 10^6$ cm^{-3} (black) to $n = 6$ cm^{-3} (white), $r_0 = 2 \times 10^{14}$m, $r_1 = 4 \times 10^{14}$m, $\gamma = 5/3$ (left) $\gamma = 1.05$ (right).

	Mass loss $M_\odot/yr$	Velocity km/s	Temperature K	Q $\dot{M}_{eq}/\dot{M}_{pole}$	β	M$_{tot}$ $M_\odot$
	Inter AA					
Phase I.	1×10^{-5}	10	100	2	1	
Phase II.	1×10^{-3}	100	100	200	20	5.6×10^{-4}
	Inter AB					
Phase I.	1×10^{-5}	10	100	2	1	
Phase II.	1×10^{-3}	100	100	200	40	2.4×10^{-4}
	Inter AC					
Phase I.	1×10^{-5}	10	100	2	1	
Phase II.	1×10^{-2}	100	100	2000	30	2.8×10^{-3}
	Inter AD					
Phase I.	1×10^{-5}	10	100	2	1	
Phase II.	1×10^{-3}	150	100	200	20	5.6×10^{-4}
	Inter AE					
Phase I.	1×10^{-5}	10	100	2	1	
Phase II.	1×10^{-4}	100	100	20	10	2.4×10^{-4}
	Inter BA					
Phase I.	5×10^{-5}	10	100	10	5	
Phase II.	1×10^{-3}	100	100	200	20	5.6×10^{-4}
	Inter Soker					
Phase I.	1×10^{-5}	10	100	2	1	
Phase II.	1×10^{-2}	100	1000	-	-	4.2×10^{-2}

Table 1: Parameters for the intermediate wind simulations. The grid size is 200×200 cells

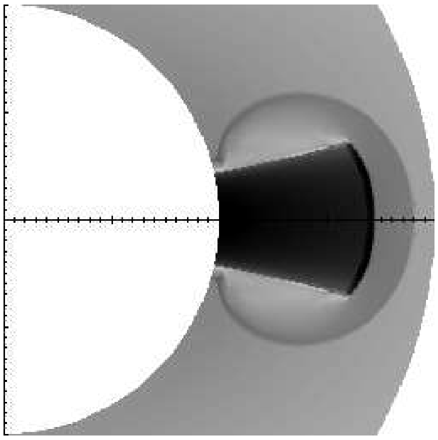

Figure 9: *The intermediate wind*, **inter Soker**, Logarithmic density plot after 50 yrs, scaling from $n = 6 \times 10^6$ cm^{-3} (black) to $n = 6$ cm^{-3} (white), $r_0 = 2 \times 10^{14}$m, $r_1 = 4 \times 10^{14}$m, $\gamma = 5/3$.

of the equator. A complete shell will also form if the density or temperature differs from the surrounding matter.

We use the equations described in section 3.4 for the intermediate wind, and some adjustments had to be made in order to avoid shocks above 10° from the equator. First of all, we assume that the velocity depends on θ, using the distribution function of eqn. 3.2. We calculate a Q_v, see eqn. 3.3–3.4, as the ratio between the velocity of the intermediate wind and the velocity of the RSG wind. The result is that the velocity of the ejected matter is equal to the surrounding gas in the polar direction, and higher at the equator. We assume the temperature does not change during the pulse. In order to get an equal mass loss in the polar direction, Q is calculated as the ratio between the RSG mass loss and the mass loss for the intermediate wind.

Six simulations were run using our method with different sets of parameters, and the result can be seen in figures 7-8. The resolution is 200 × 200 grid cells, the inner radius is 2×10^{14}m and the outer radius is 4×10^{14}m. The close outer radius gives a much higher resolution for this phase than in Sokers simulations. The parameters for each simulation can be found in table 1, and the simulations have been named using the prefix **inter** and a suffix of two letters to connect the parameter values with the plots.

One effect which could have a strong impact is radiative cooling. All the simulations where therefore re-run with $\gamma = 1.05$, a trick used by Blondin & Lundqvist (1993) and many others.[3]

[3]Martin & Arnett (1995) investigated the effect of radiative cooling in the interactive winds model more carefully, and as their results agreed well with those of Blondin &

The plots show the grid after 50 years, the left picture with $\gamma = 5/3$ and the right with $\gamma = 1.05$. The simulations show more or less the same thing; a pulse of dense intermediate wind moving fast in the equatorial direction and pushing an even denser shell of shocked intermediate wind ahead of it. Surrounding the whole structure is a shell of shocked RSG wind, due to the high velocity of the intermediate wind, which has the cross-section of a bow shock. Bow shocks are generally found when simulating polar jets, in our case the shock takes the form of a disk when rotated around the symmetry axis. With radiative cooling the gas in front of the expanding structure cools of before any prominent shell can form and this has implications that will become appearent in the next section.

It seems like the density distribution for the initial RSG wind is of small importance for the structure (**inter BA**, fig.8), a high density in the equatorial region slows the structure down but hardly changes its shape. The shape of the structure follows the distribution function for the density and velocity, and as the pulse has much higher density and velocity than the RSG wind it evolves pretty much unperturbed by the surrounding gas.

For comparison a simulation was run using Sokers scheme for the intermediate wind. With Sokers scheme the intermediate wind forms a cone of dense matter, which grows radially rather than along the equatorial direction (see fig.9), which may be the key property that gives the horse-shoe cross-section. The plot should be compared with **inter AC**, fig.7 (bottom left). An obvious conclusion from comparing the two cases is that the velocity distribution sets the shape and further evolution of the pulse. Thus the implementation of the intermediate wind is the very basis upon which the whole case rests. We have chosen to focus on our description of the second phase in the following simulations, but as the model for the outer rings is based upon the results of Sokers simulations in 1989 both methods must be tested.

4.2 The red wind

The intermediate wind has been investigated in the previous section, the time has now come to see what effect the resumed slow wind has and how the pulse itself evolves. Nine different sets of parameter values were tested with and without radiative cooling. The resolution was 200×200 grid cells which, with an inner radius of 2×10^{14}m, gives a maximal outer radius of 4×10^{15}m if phase II is to be resolved. The parameters for the test runs can be found in table 2 and plots in Figures 11–13. The top picture shows the grid after 750 years and the picture underneath it shows the grid after 2000 years. The two bottom pictures are obtained with the same set of parameters, but using radiative cooling. Two simulations have been run using Sokers

Lundqvist the approximation should be accurate enough.

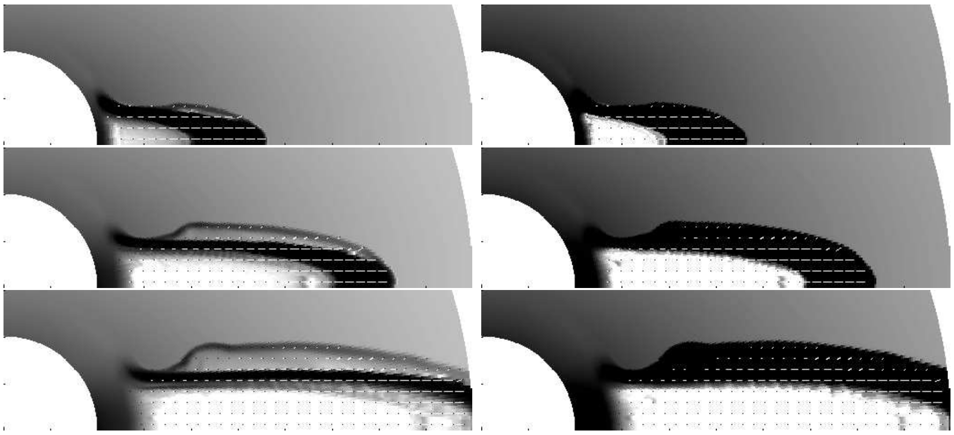

Figure 10: *The formation of the three shells.* Logarithmic plots of density(left) and pressure(right) for the evolution of **lrIX** at $t = 68, 163, 262$ yrs, scaling from $n = 3 \times 10^5$ cm^{-3}, $p = 1 \times 10^{-10}$N m^{-2} (black) to $n = 600$ cm^{-3}, $p = 5 \times 10^{-13}$N m^{-2} (white), $r_0 = 2 \times 10^{14}$m, $r_1 = 1 \times 10^{15}$m, $\gamma = 1.05$. Velocity arrows drawn for velocities larger than 10 km s$^-1$

distribution function for the intermediate wind, one with $\gamma = 5/3$ and one with $\gamma = 1.05$, the results are plotted in fig.14. The structure created during the intermediate wind phase goes through drastic changes. The ejected material of the merger moves outwards very fast, and piles up behind the shock at the tip of the expanding structure, see fig.10. The region behind the shock is cleared, and the resumed RSG wind is too slow to to fill up the rapidly growing gap. The region of shocked intermediate wind gets its shape from the velocity of the intermediate wind, which gives a trail of slower moving material forming a dense, high pressured shell. This does not happen using Sokers scheme of a constant velocity for the intermediate wind, compare fig.13 with fig.14. The extremely low pressure of the empty region along the equator eventually makes the overlying material expand towards the equator. This in turn creates yet another shell, which is most appearent in the low γ simulations, see for example the two bottom plots in fig.12. The shell from the bow shock still surrounds the whole structure, and become the outer egde of the horse-shoe torus.

Radiative cooling is vital for the model to work as the bow shock which gives the horse-shoe torus blows up to huge proportions without cooling. The most drastic example of this can be found in fig.14 (2nd row) where the structure has closed upon itself and is no longer a torus.

With radiative cooling and Sokers description of the intermediate wind we obtain the famous hollowed horse-shoe torus (fig.14, 3rd & 4th row). The shell is very dense and thin, but tends to close at the equator rather than having well defined end-points. So far there is no tendency towards clumping as reported by Soker (1989) – the density of the shell decreases smoothly as the width radially increases.

The θ dependence on the velocity leads, as described above, to a quite different structure. Instead of one thin, dense shell we obtain three shells. The two outer shells are connected in high density end-points and together form the horse-shoe torus. The width of the cross-section (i.e the distance between the inner and outer radius) is much larger than the thin shell obtained using Sokers scheme, and has the form of an elongated horse-shoe with density concentrated at the edges.

A high asymmetry for the mass loss in the first phase will make it more difficult for the structure to expand in the equatorial direction. This is demonstrated in fig.11 where the density of the RSG wind is both higher and much more concentrated in the equatorial plane. The effect is most apparent in the case without radiative cooling. The horse-shoe evolves into a heart shaped structure, with its end-points moving towards the pole. If the end-points lie within the inner ring, as observed from above, the result will be a large outer ring and two small inner rings. Therefore low asymmetry for the first phase wind is assumed in the following simulations, consistent with the model in which the assymetry is introduced by the merger.

As can be seen, an outer radius of 4×10^{15}m is in some cases not enough to keep the whole structure on the grid for 2000 years. This must be considered when doing the large scale simulations.

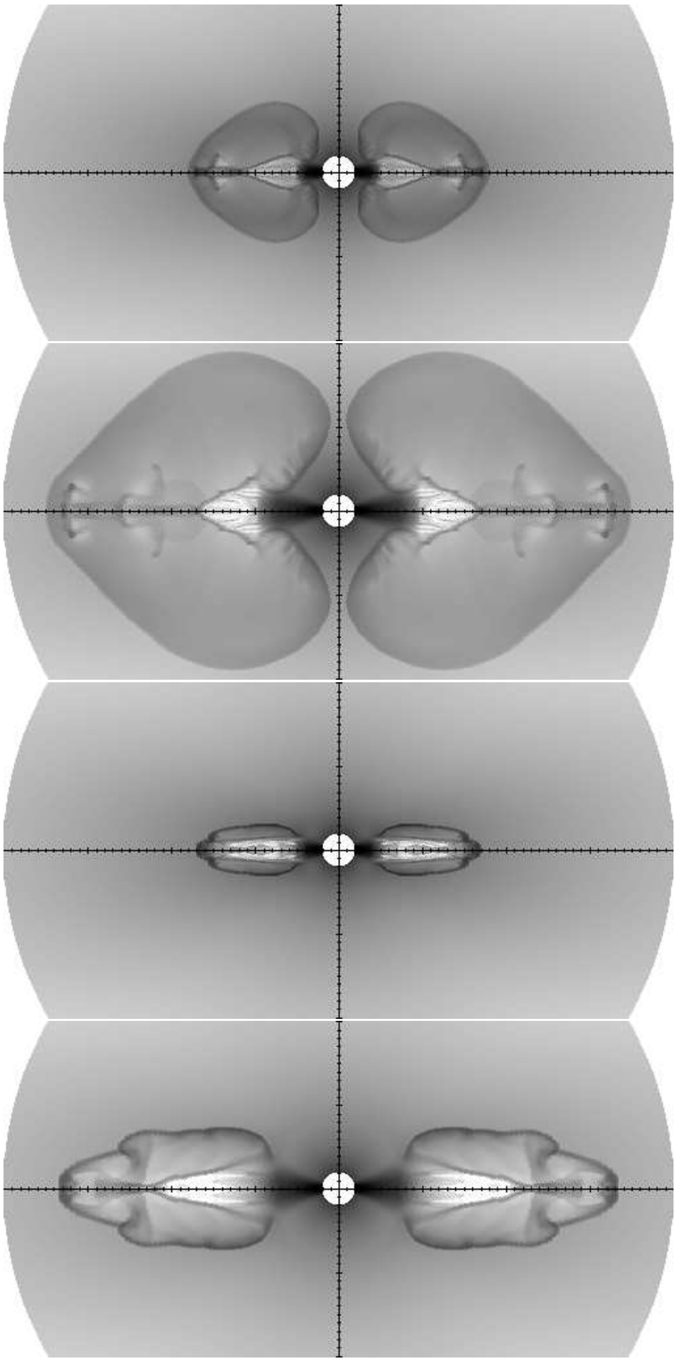

Figure 11: *Slow wind.* Logarithmic plots of density for **lrI** at $t = 750$ yrs. and $t = 2000$ yrs, scaling from $n = 6 \times 10^6$ cm^{-3} (black) to $n = 60$ cm^{-3} (white), $r_0 = 2 \times 10^{14}$m, $r_1 = 4 \times 10^{15}$m, $\gamma = 5/3$ (top plots), $\gamma = 1.05$ (bottom plots).

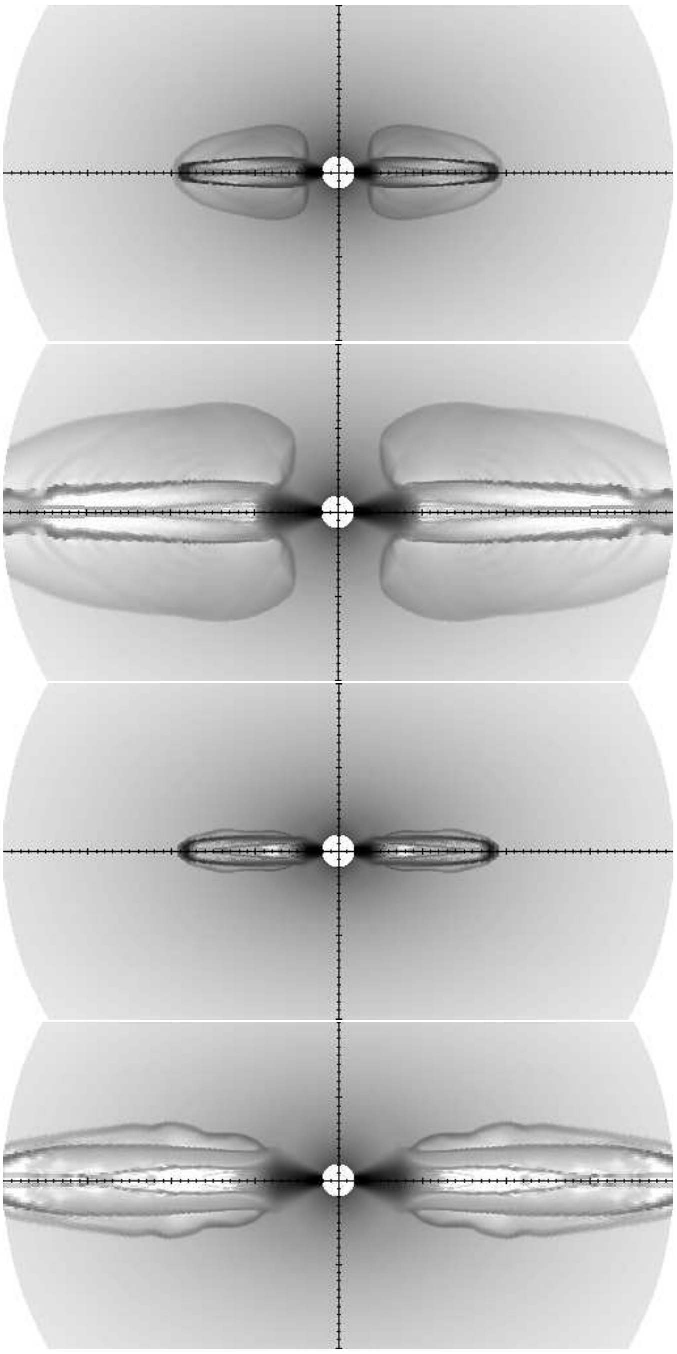

Figure 12: *Slow wind.* Logarithmic plots of density for **lrIV** at $t = 750$ yrs. and $t = 2000$ yrs, scaling from $n = 6 \times 10^6$ cm^{-3} (black) to $n = 60$ cm^{-3} (white), $r_0 = 2 \times 10^{14}$m, $r_1 = 4 \times 10^{15}$m, $\gamma = 5/3$ (top plots), $\gamma = 1.05$ (bottom plots).

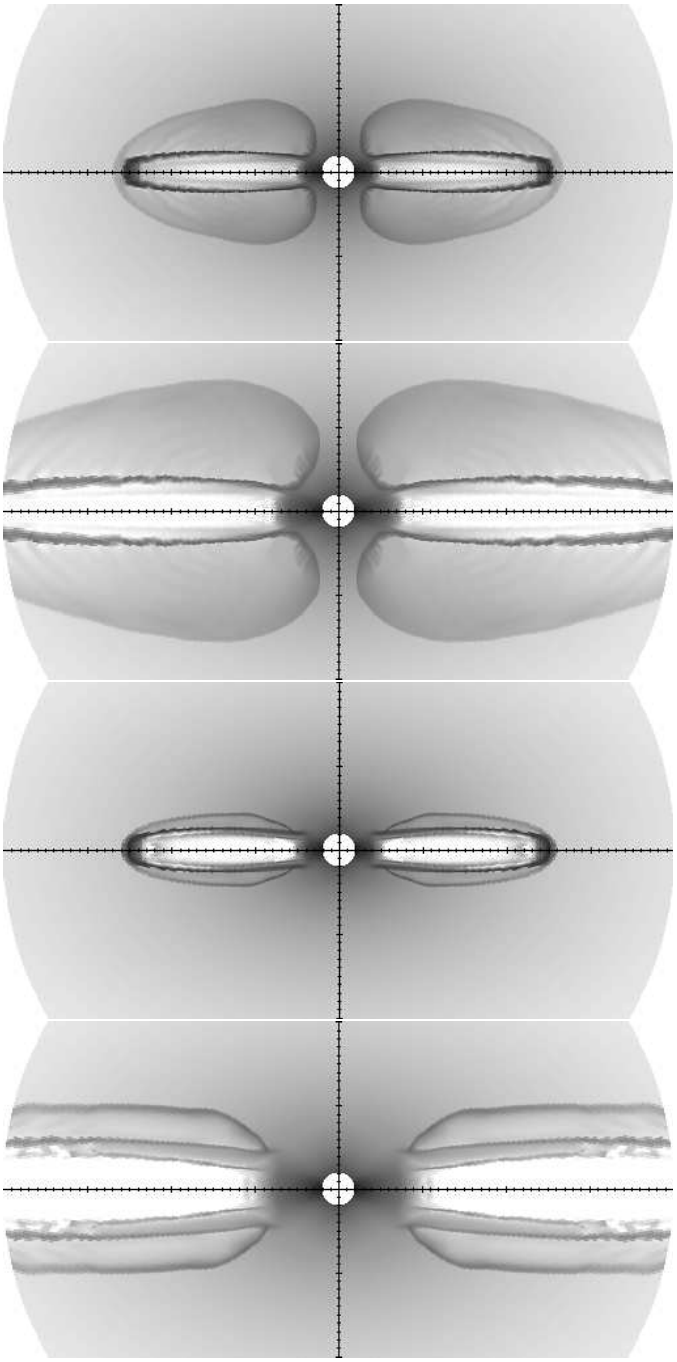

Figure 13: *Slow wind.* Logarithmic plots of density for **lrIX** at $t = 750$ yrs. and $t = 2000$ yrs, scaling from $n = 6 \times 10^6$ cm^{-3} (black) to $n = 60$ cm^{-3} (white), $r_0 = 2 \times 10^{14}$m, $r_1 = 4 \times 10^{15}$m, $\gamma = 5/3$ (top plots), $\gamma = 1.05$ (bottom plots).

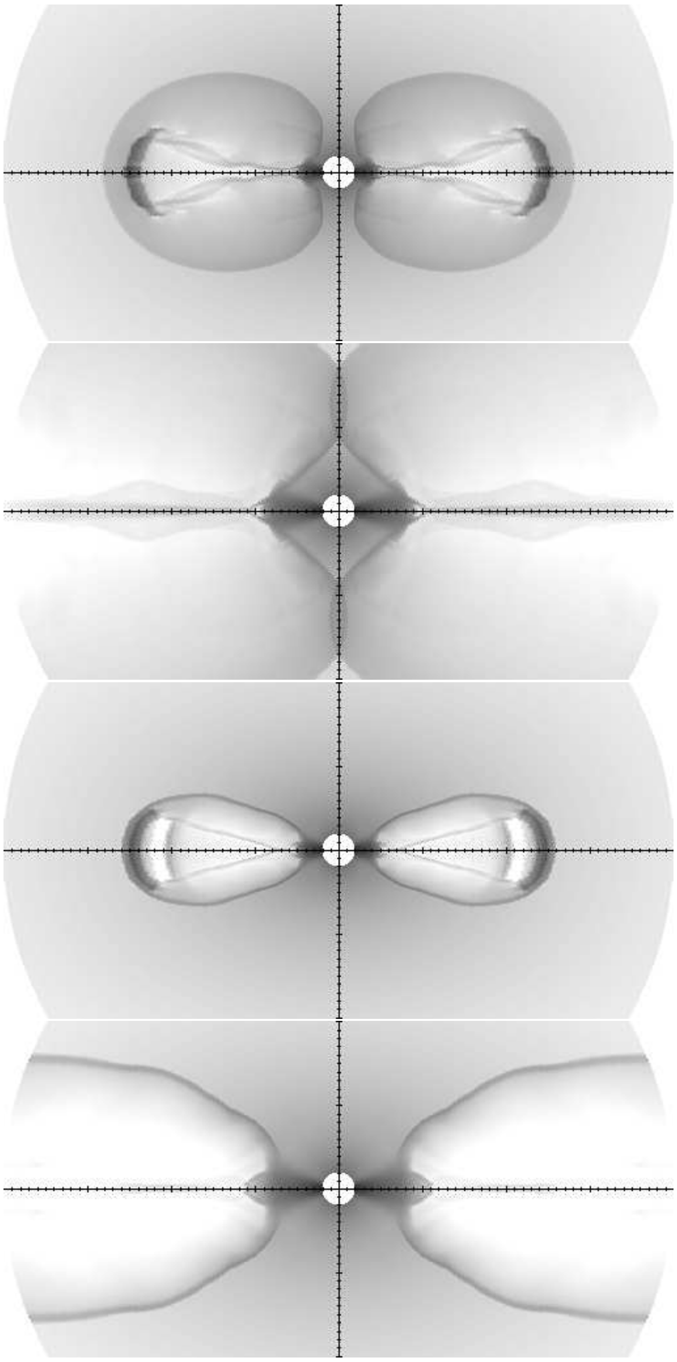

Figure 14: *Slow wind.* Logarithmic plots of density for **lrSoker** at $t = 750$ yrs. and $t = 2000$ yrs, scaling from $n = 6 \times 10^6$ cm^{-3} (black) to $n = 60$ cm^{-3} (white), $r_0 = 2 \times 10^{14}$m, $r_1 = 4 \times 10^{15}$m, $\gamma = 5/3$ (top plots), $\gamma = 1.05$ (bottom plots).

	Mass loss $M_{\odot}/yr$	Velocity km/s	Temperature K	Q $\dot{M}_{eq}/dotM_{pole}$	β
	lrI				
Phase I.	5×10^{-5}	10	100	5	3
Phase II.	2×10^{-3}	100	100	200	20
Phase III.	2×10^{-4}	10	100	20	15
	lrII				
Phase I.	1×10^{-5}	10	100	2	1
Phase II.	1×10^{-3}	70	100	200	30
Phase III.	2.5×10^{-4}	10	100	50	15
	lrIII				
Phase I.	1×10^{-5}	10	100	2	1
Phase II.	1×10^{-3}	100	100	200	30
Phase III.	3×10^{-5}	10	100	6	5
	lrIV				
Phase I.	1×10^{-5}	10	100	2	1
Phase II.	1×10^{-2}	70	100	2000	30
Phase III.	2.5×10^{-4}	10	100	50	15
	lrV				
Phase I.	1×10^{-5}	10	100	2	1
Phase II.	1×10^{-2}	1.5×10^{5}	100	2000	30
Phase III.	2.5×10^{-4}	10	100	50	15
	lrVI				
Phase I.	1×10^{-5}	10	100	2	1
Phase II.	1×10^{-2}	70	100	2000	50
Phase III.	2.5×10^{-4}	10	100	50	15
	lrVII				
Phase I.	1×10^{-5}	10	100	2	1
Phase II.	1×10^{-2}	70	100	2000	30
Phase III.	5×10^{-5}	10	100	10	5
	lrVIII				
Phase I.	1×10^{-5}	5	100	2	1
Phase II.	1×10^{-2}	70	100	2000	30
Phase III.	1×10^{-4}	5	100	20	10
	lrIX, **lrIXlowR0**				
Phase I.	1×10^{-5}	5	100	2	1
Phase II.	1×10^{-2}	100	100	2000	15
Phase III.	3×10^{-5}	5	100	6	4
	lrSoker				
Phase I.	1×10^{-5}	10	100	2	1
Phase II.	1×10^{-2}	100	1000	-	-
Phase III.	1×10^{-4}	10	100	20	10

Table 2: Parameter values for the slow wind simulations. The grid size is 200×200 cells.

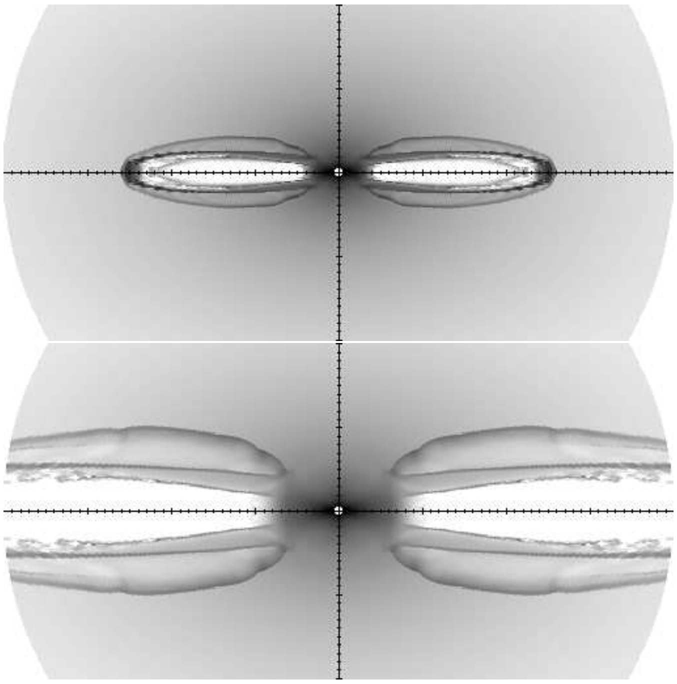

Figure 15: *Slow wind.* Logarithmic plots of density for **lrIXlowR0** at $t =$ 818 yrs. and $t = 2068$ yrs, scaling from $n = 6 \times 10^6$ cm^{-3} (black) to $n = 60$ cm^{-3} (white), $r_0 = 2 \times 10^{14}$m, $r_1 = 4 \times 10^{15}$m, $\gamma = 1.05$.

With an inner radius of 2×10^{14}m, one has a white area within which one has no information. Thus the intermediate wind starts its interaction with the RSG wind at the inner radius, which of course is not the true case. The way around this problem is to use what is called an expanding grid. One starts with a small inner radius, tracing the shock front of the expanding structure. As the shock progresses, the grid is recalculated by extrapolation to a grid with a larger inner and outer radius keeping the shock front at the same position. This way the development of the simulation can be followed from a very small radius to great distances, without increasing the grid resolution. Unfortunately there was no time to implement this function. In order to see how the inner radius affect the evolution of the structures, a simulation was run using an inner radius of 5×10^{13}m, $\gamma = 1.05$ and the same parameters as used for **lowresIX** fig.13. The simulation was halted when the shock of the intermediate wind reached the same radius as **lowresIX**, and is shown in fig.15. As can be seen the resulting structure is very much alike **lowresIX**, showing that the inner radius has no large scale effect on the long term evolution of the flow.

4.3 The blue wind

As the velocity of the blue wind is much higher than the previous winds, the time step decreases which makes the simulations painfully slow. Further more, the blue wind must last for several thousand years in order to blow the less dense material off the grid. Thus the time required for a simulation is vastly increased and easily takes days to run.

The standard values for the BSG wind from the simulations of Blondin & Lundqvist are $\dot{M} = 2 \times 10^{-6}$ $M_{\odot}$/s, $v = 300$ km/s and $T = 10000$ K. As mentioned in section 2.2.2 these values are out of date, the mass loss in the ionizing models is at least a factor 10 lower and the wind velocity is higher. The code used for this model does not include ionization, and it seems therefore unnecessary to use the latest values. The interacting wind scheme results in similar density structures as the ionizing models, though giving higher expansion velocities. The argument to continue with the blue wind is thus that the structure obtained with a dense blue wind will be more or less comparable to the effect of ionization.

When the progenitor shrinks to a BSG its spin increases proportionally, which may give it an asymmetric mass loss. Six simulations have been run with a resolution of 300×300 grid cells and an outer radius of 6×10^{15}. The first (**mrIV_I**) feature a spherical blue wind with the standard values, while the blue wind is asymmetric in the second simulation (**mrIV_III**). Both were first run without radiative cooling, which may seem foolish as cooling gives the horse-shoe torus a very different shape. However, effects that are difficult to see using cooling might be more obvious without cooling, and the simulations were run to give a better understanding of the evolution. The two simulations were re-run with $\gamma = 1.05$, consequently named **mrCIV_I** and **mrCIV_III**. The parameters for the first three phases where taken from the fourth low resolution simulation (**lrIV**), as these gave a horse-shoe structure most like Soker's description. The parameters for the third phase are quite extreme in these simulations, and the area between the inner ring and the horse-shoe end-points is quite dense. A possible consequence is that the blue wind then cannot separate the two, as it does not "leak" into the hollowed horse-shoe torus. Therefore two simulations were run with the parameters of **lrIX**, where the parameters for the third phase are those derived by Blondin & Lundqvist for the RSG phase. Also, the steepness parameter β was reduced for the intermediate wind, giving a more open horse-shoe structure. Radiative cooling was assumed, and both a spherical (**mrCIX_I**) and an asymmetric (**mrCIX_III**) blue wind were tested. In the final simulation, **mrSCX**, Sokers scheme for the second phase was applied, this also with radiative cooling. The RSG wind was active for 1000 years.

The results are quite discouraging. The simulations were stopped when the shell created by the blue wind reached the end of the grid. At this point the density is concentrated in several areas, which due to the assumed axi-

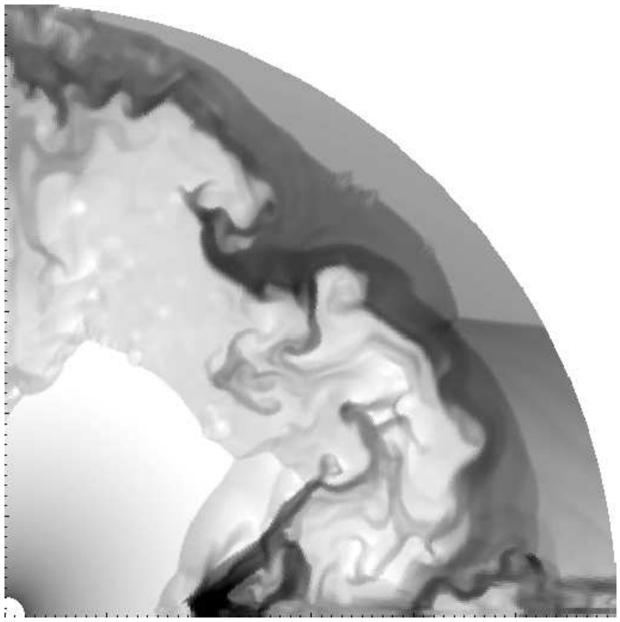

Figure 16: *Blue wind.* Logarithmic plot of density for **mrIV_I** at $t = 4187$ yrs. scaling from $n = 6 \times 10^3$ particles cm^{-3} (black) to $n = 3$ particles cm^{-3} (white), $r_0 = 2 \times 10^{14}$m, $r_1 = 6 \times 10^{15}$m, $\gamma = 5/3$

symmetry create multiple rings. The evolution of the simulations varies but the common event is what previously was found; the formation of the inner ring with a diagonal wall decreasing in density. However, all the possible candidates for the outer rings lie either at, or within, the radius of the inner ring when observed from above. This will give two small rings and a large outer ring.

In the simulations without radiative cooling, called **mrIV_I** (fig.16) and **mrIV_III** (fig.17), the horse-shoe torus expands, making the surrounding shells low enough in density for the fast blue wind to punch a hole through the end-points and leak into the horse-shoe. This splits up the previously connected shells, the lower shell is pushed downwards toward the equator while the upper tends to move towards the pole. One intresting detail is that the blue wind overtakes and enclose the dense region of the inner ring, as it flows into the horse-shoe structure.

Moving on to the more important low γ simulations, the evolution is quite different. With the parameters used in **mrCIV_I** (fig.18) and **mr-CIV_III** (fig.19) there is a very dense region at the equator from the highly asymmetric intermediate and red wind. As the expanding bubble of shocked BSG wind reaches the region, the equatorial wind is forced polewards. This produce a bulge in the bubble which grows dramatically in size, and cusps

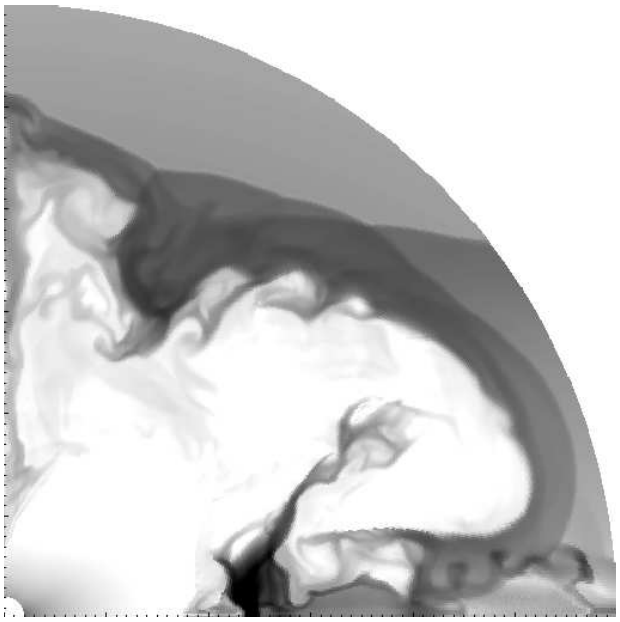

Figure 17: *Blue wind.* Logarithmic plot of density for **mrIV_III** at $t = 5512$ yrs. scaling from $n = 6 \times 10^3$ particles cm^{-3} (black) to $n = 3$ particles cm^{-3} (white), $r_0 = 2 \times 10^{14}$m, $r_1 = 6 \times 10^{15}$m, $\gamma = 5/3$

are formed. An asymmetry for the blue wind only makes matters worse, as the deflected wind gets a higher momentum which increases the effect. Cusps form in the same regions in the simulations of Blondin & Lundqvist as well as in the simulations of Martin & Arnett (1995), and tend to flatten out and merge with the shell of shocked BSG wind later on. No good candidates for the outer rings form in the **mrCIV** simulations. The blue wind seems unable to do much to the dense horse-shoe torus, the end-points are at best pushed somewhat into the horse-shoe and not at all swept up as predicted. This set of parameters is thereby disqualified.

With the more gentle, and reasonable, parameter-set of **mrCIX** things look better. The evolution of this simulation can be found in figures 21–22, the pictures are from now on referred to as a, b, c, d and e in chronological order. A second simulation was run using an aspherical blue wind, which can be seen in fig.20. The structure is elongated in the equatorial direction, giving slightly lower polar velocities, but is otherwise analogous to the spherical case.

(a): The blue wind has just made its appearance on the grid. The equatorial elongation of the horse-shoe torus has slowed down and the structure is from now mainly expanding radially.

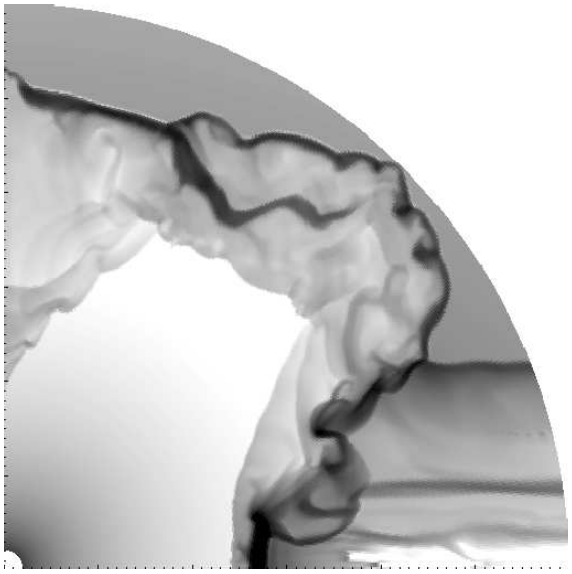

Figure 18: *Blue wind.* Logarithmic plot of density for **mrCIV_I** at $t = 6287$ yrs. scaling from $n = 6 \times 10^3$ particles cm^{-3} (black) to $n = 3$ particles cm^{-3} (white), $r_0 = 2 \times 10^{14}$m, $r_1 = 6 \times 10^{15}$m, $\gamma = 1.05$

(b): The bubble of shocked blue wind has reached the horse-shoe structure. At this point the hour glass tendency is getting observable, as the dense region from the asymmetric RSG wind impedes expansion in the equatorial direction.

(c): The expansion of the bubble is slowed down where it intersects the two outer shells, and slowly penetrates the horse-shoe end-point. At the equatorial axis a tunnel through the bubble is beginning to form. This is most probably due to a numerical error from pressure correction or smoothing, the axis is a very sensitive area where errors have the largest impact. As the inner ring structure is somewhat ruined by this, we turn our full attention to the outer rings.

(d): A multiple of cusps and bulges have formed. The blue wind streams in between the shells, and a dense region is formed from swept up outer shell material. This region will be the best candidate on the grid for the outer rings.

(e): The cusps from interaction with the inner shells move outwards, while the dense region from the outer shell is left behind. The density of this region is more than 100 times the surrounding gas, and is interacting almost directly with the blue wind rather than with the inner shock of the expanding bubble. The velocity is roughly 14 km/s and seems

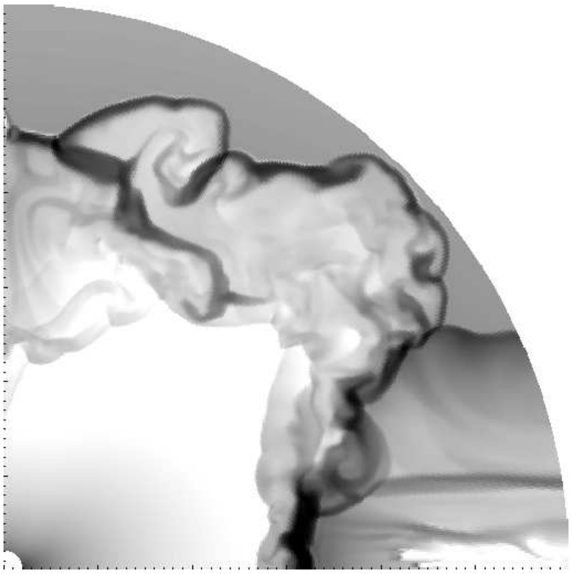

Figure 19: *Blue wind.* Logarithmic plot of density for **mrCIV_III** at $t = 7469$ yrs. scaling from $n = 6 \times 10^3$ particles cm^{-3} (black) to $n = 3$ particles cm^{-3} (white), $r_0 = 2 \times 10^{14}$m, $r_1 = 6 \times 10^{15}$m, $\gamma = 1.05$

radial, although the high turbulence of the area makes this more a guess than a fact. What is left of the inner ring is expanding with 20 km/s, hence the outer ring lags behind, and will end up inside the inner ring given more time. Recently published values for the expansion velocities (Crotts & Heathcote, 2000) are 26 km/s vs. 23 km/s for the outer rings and 10.5 km/s for the inner ring. Sokers model was designed to give slow expansion velocities, as discussed in section 2.3, and the high expansion velocity of the inner ring is a well known problem ever since the very first simulations of the interactive winds model. However, the combination of too slow expansion for the outer rings and the too high velocity of the inner ring renders the situation quite hopeless.

The most important test of the model is made in **mrSCX_I**. The model is, as mentioned many times before, built on the results of Soker (1989) where the velocity of the intermediate wind is constant over θ. The evolution of this simulation can be found in figures 23–24. The pictures are named a, b, c and so forth, like in the previous paragraph.

(a): As can be seen the area between the horse-shoe end points (which are very close to the equator) and the inner ring is very dense. This forces the blue wind pole-wards and the hour glass tendency is very appearent after just a few hundred years.

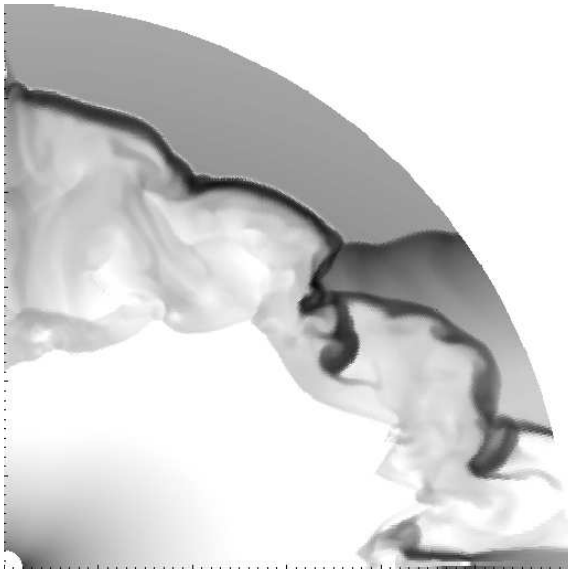

Figure 20: *Blue wind.* Logarithmic plot of density for **mrCIX_III** at $t =$ 7713 yrs. scaling from $n = 6 \times 10^3$ particles cm^{-3} (black) to $n = 3$ particles cm^{-3} (white), $r_0 = 2 \times 10^{14}$m, $r_1 = 6 \times 10^{15}$m, $\gamma = 1.05$

(b): Like in **mrCIV_I** and **mrCIV_III** a bulge is formed in the expanding bubble, where the blue wind climbs pole-wards over the horse shoe shell.

(c): A prominent cusp has formed at the bulge. The blue wind has broken through the shell of the horse-shoe, and leaks into the torus.

(d): A long tail has derived from the cusp. The horse-shoe shell is being swept up into a dense region, while the inner ring is overtaken by the blue wind.

(e): The dense region of swept up horse-shoe shell endures, and is growing in density. The ratio to the surrounding gas is much more than 100, and makes the region the best candidate for the outer ring so far. It expands with a velocity of 14 km/s, compared to 16 km/s for the inner ring.

The model seems to be too good at producing low velocity outer rings, none of the simulations have given outer rings with higher velocity than the inner ring. At this stage the inner ring has reached a radius of 3×10^{15}m. which is halfway to its present radius. The probability that the outer rings should reverse the trend of lagging behind, and accelerate enough to reach a radius twice that of the inner ring is infinitesimal.

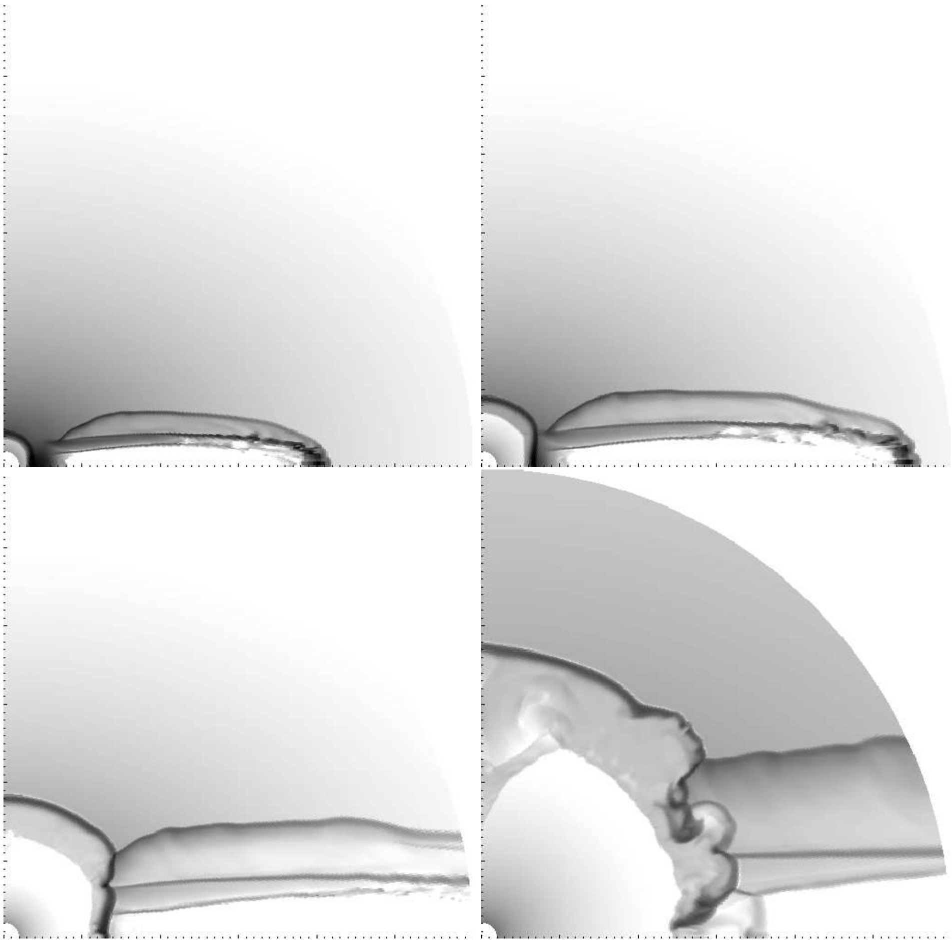

Figure 21: *Blue wind.* Logarithmic plot of density for **mrCIX_I** at $t = 348$ yrs (tl), $t = 940$ yrs (tr), $t = 2126$ yrs (bl), $t = 4496$ yrs (br), $n = 6 \times 10^5$ particles cm^{-3} (black) to $n = 600$ particles cm^{-3} (br:$n = 60$ particles cm^{-3}) (white), $r_0 = 2 \times 10^{14}$m, $r_1 = 6 \times 10^{15}$m, $\gamma = 1.05$

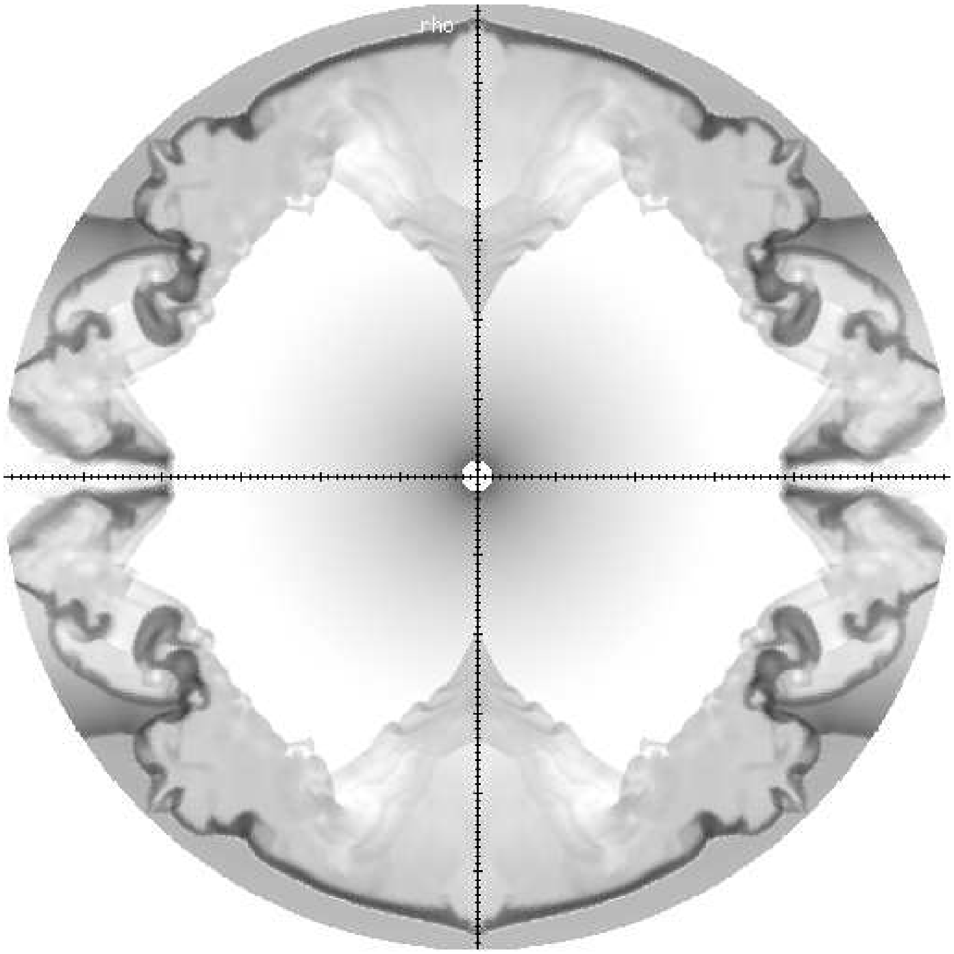

Figure 22: *Blue wind.* Logarithmic plot of density for **mrCIX_I** at $t = 6866$ yrs $n = 6 \times 10^5$ particles cm^{-3} (black) to $n = 30$ particles cm^{-3} (white), $r_0 = 2 \times 10^{14}$m, $r_1 = 6 \times 10^{15}$m, $\gamma = 1.05$

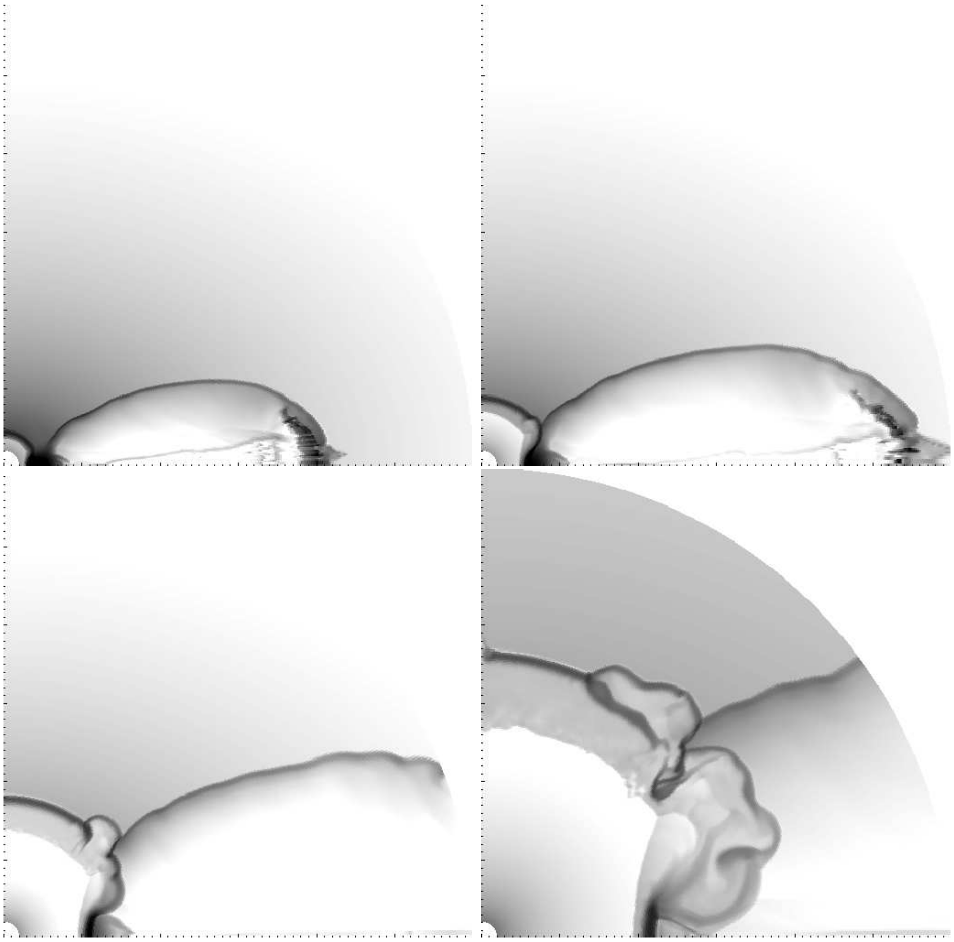

Figure 23: *Blue wind.* Logarithmic plot of density for **mrSCX_I** at $t = 343$ yrs (tl), $t = 935$ yrs (tr), $t = 2120$ yrs (bl), $t = 4491$ yrs (br), $n = 6 \times 10^5$ particles cm^{-3} (black) to $n = 600$ particles cm^{-3} (br:$n = 60$ particles cm^{-3}) (white), $r_0 = 2 \times 10^{14}$m, $r_1 = 6 \times 10^{15}$m, $\gamma = 1.05$

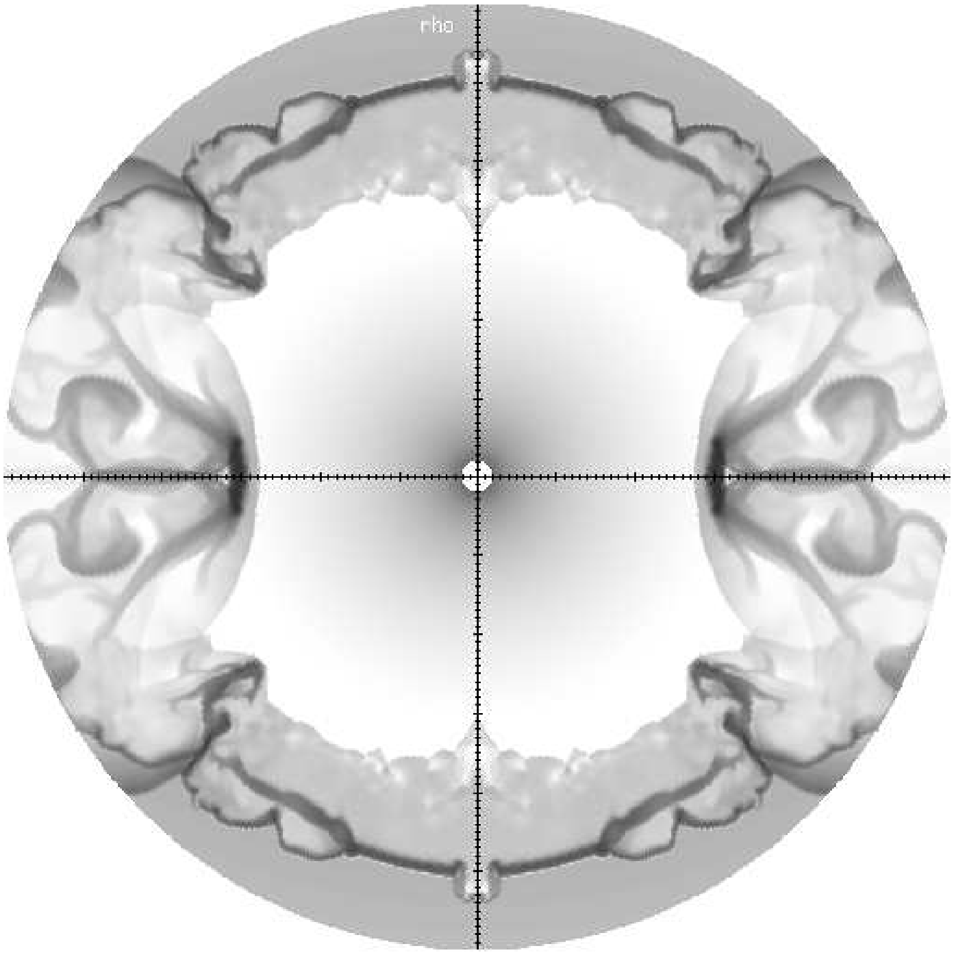

Figure 24: *Blue wind.* Logarithmic plot of density for **mrSCX_I** at $t = 6269$ yrs $n = 6 \times 10^5$ particles cm^{-3} (black) to $n = 30$ particles cm^{-3} (white), $r_0 = 2 \times 10^{14}$m, $r_1 = 6 \times 10^{15}$m, $\gamma = 1.05$

	Mass loss $M_\odot/yr$	Velocity km/s	Temperature K	Q $\dot{M}_{eq}/\dot{M}_{pole}$	β
	mrIV_I, mrCIV_I				
Phase I.	1×10^{-5}	10	100	2	1
Phase II.	1×10^{-2}	100	100	2000	30
Phase III.	2.5×10^{-4}	10	100	50	15
Phase IV.	1×10^{-6}	300	10000	1	1
	mrIV_III, mrCIV_III				
Phase I.	1×10^{-5}	10	100	2	1
Phase II.	1×10^{-2}	100	100	2000	30
Phase III.	2.5×10^{-4}	10	100	50	15
Phase IV.	1×10^{-6}	300	10000	5	3
	mrCIX_I				
Phase I.	1×10^{-5}	10	100	2	1
Phase II.	1×10^{-2}	100	100	2000	15
Phase III.	3×10^{-5}	10	100	6	3
Phase IV.	1×10^{-6}	300	10000	1	1
	mrCIX_III				
Phase I.	1×10^{-5}	10	100	2	1
Phase II.	1×10^{-2}	100	100	2000	15
Phase III.	3×10^{-5}	10	100	6	3
Phase IV.	1×10^{-6}	300	10000	5	3
	mrSCX_I				
Phase I.	1×10^{-5}	10	100	2	1
Phase II.	1×10^{-2}	100	1000	-	-
Phase III.	1×10^{-4}	10	100	20	10
Phase IV.	1×10^{-6}	300	10000	1	1

Table 3: Parameter values for the medium resolution blue wind simulations. The grid size is 200×200 cells.

5 Conclusions

The model suggested by Soker does produce the rings, with one great flaw: the dense regions which are supposed to give the outer rings end up inside the inner ring resulting in one outer ring and two inner rings. The slow expansion of the outer rings was an intended property of the model, but is in contradiction with the recently measured velocities which are at least twice as high. As has previously been found, the inner ring gets a much too high velocity with the interacting winds model.

The results of the simulations depends notably on the second phase, where the short pulse of matter from the merger is ejected. A velocity constant over θ for this intermediate wind results in a very different structure than with an angle dependence. We therefore draw the conclusion that the shape of the horse shoe torus depends mostly on the shape of the velocity distribution and not just on the amount of energy released. The model thus needs a more physical description of the second phase.

Radiative cooling is absolutely necessary for the model to work, without which the horse-shoe torus expands too much to be swept up by the blue wind. The result is instead a large, medium-dense area too close to the polar axis, which cannot serve as a candidate for an outer ring.

The recent opinion is that ionization of the RSG wind rather than interaction with the BSG wind give rise to the hydrodynamical motions forming the inner ring. As the model does not include ionization, it is impossible to say what the result of an intermediate wind would really be. The structures obtained with ionization are similar to those from interactive wind models, but it is uncertain if an expanding shell due to ionization will sweep up the end-points of the horse-shoe like the dense blue wind.

6 Acknowledgements

The author would like to thank Garrelt Mellema for his supreme guidance and for treating me like a fellow collegue rather than a student, Peter Lundqvist who has been a great source of inspiration and who has given me a good insight into the up-to-date theories of '87A, Sara Bergenius and Jan Duracz for their many suggestions and help with this report, Patrik Usher who helped me set up Linux and without whom I would still be at square one, and to all you other friends and relatives who have put up with my whining and short temper during the last months.

Ps. A warm regard to Crotts and Heathcote for giving a final blow to the already mortally wounded model, thus totally relieving me and mr. Soker for the responsibility of the confusing results in this report.

References

[1] Blondin M., Lundqvist P., *1993 ApJ*, **405**, 337

[2] Burrows C. et al., *1995 ApJ*, **452**, 680

[3] Chevalier R., *2000, in 'SN 1987A: Ten Years After, The Fifth CTIO/ESO/LCO Workshop'*, eds. M. Phillips & N. Suntzeff, in press

[4] Chevalier R., Dwarkadas V., *1995 ApJ*, **452**, L45

[5] Crotts A., Heathcote S., *2000 ApJ*, **528**, 426

[6] Eulderink F., Mellema G., *1995 A&AS*, **110**, 587

[7] Lloyd H.M., O'Brien T.J. & Kahn F.D., *1995 MNRAS*, **273**, L19

[8] Lundqvist P., *1999 ApJ*, **511**, 389

[9] Martin C., Arnett D., *1995 ApJ*, **447**, 378

[10] Mellema G., Eulderink F. & Icke V., *1991 A&A.*, **252**, 718

[11] Meyer F., *1997 MNRAS*, **285**, L11

[12] Panagia N., et al., *1996 ApJ*, **459**, L17

[13] Roe P.L., *1981, in: Proceedings Seventh Int. Conf. Num. Meth. in Fluid Dyn., eds. W.C. Reynolds, R.W. MacCormack (Springer Verlag, Berlin)*

[14] Soker N., *1999 MNRAS*, **303**, 611

[15] Soker N., *1989 ApJ*, **340**,927

[16] Washimi H., Shibata S., Mori M., *1996 PASJ*, **48**, 23W

A Appendix:Description of the interface program

A.1 Introduction

In addition to the program doing the actual calculations I have developed a graphical interface from which you control the simulation. It is written in C++, using the basic X11 libraries. Writing all menu- and button-functions from scratch required a lot of code, but in turn gave a high aesthetic freedom which I have abused to the best of my ability.

This initially small side-project I took upon myself became a big time-consumer into which many hours went from the real project. But, I think it turned out rather nice, and I hope someone will find it amusing to play around with.

Besides from plotting different graphs from the simulation, the interface allows you to set the parameters used in the simulation as well as recording a movie or creating a rendered image of the grid. The main screen, which appears as you start the program, features a row of menu buttons and an area for plotting. When you move the mouse over the plots, the corresponding cell data will be displayed in a box at the bottom.

A.2 Menu buttons

A.2.1 Start

Yes, this button starts/restarts the simulation. As time was short, there was no time to learn and implement the client features of X-lib. Therefore you loose all contact with the interface once you press this button, until the simulation for some reason is halted.

A.2.2 Quit

Don't press this button unless you want to quit.

A.2.3 Draw

Draw 1D One dimensional graphs are plotted for different angles, along straight radial lines, the darkest colour for the equator and then scales brighter the nearer you come the pole.

Draw 2D One quadrant of the two dimensional plane is plotted.

Draw 2D full Same as 2D, only that the quadrant is mirrored to produce a full circle grid.

Draw 3D A quite useless, but nice looking, function giving 3-D graphs with the intensity of a cell acting as the third dimension.

All, Density, Velocity, Pressure, Temperature Whether you want to plot a full screen with just a single quantity or a split screen with all four.

Cartesian Using cartesian coordinates when showing the grid will give a rectangular plot.

Polar To plot the grid with polar coordinates, i.e the way the grid really looks.

Arrows Draws lines showing the direction of the gas velocity, the black dot marks the front of the “arrow”.

A.2.4 Set

Initial Opens a screen where you can set all parameters used in the simulation. You click on the white square under the name, and enter the value you want. Observe that there is no cursor, but the label of a selected square will get a different colour. Press space to jump to the next square.

meshR, meshTheta The size of the grid. Doubling the resolution gives runtimes 8 times higher.

gamma The gamma coefficient, initially set to 5/3 corresponding to an ideal gas. Lowering close to 1 will give an approximation of radiative cooling.

super bee 1,2 The maximum value is 2.0 and the minimum 1.0, the higher value the sharper shock discontinuities. Mess with these if the simulation behaves badly.

inner R, outer R The inner and outer radius of the grid (m).

The following two rows of parameters determines the shape of the previous and active wind. The first row contains the parameters for the previous, initial wind, the second row the ones for the active wind.

mass loss The mass loss of the star ($M_\odot$/yr).

velocity The wind velocity (m/s).

temperature The temperature of wind (T).

q The mass loss ratio between the pole and the equator.

β The steepness parameter of the distribution function.

The use of these are explained somewhat further in section A.3

pressure wind, shocked wind, velocity wind The inflow condition for the active wind.

zoom R, zoom Theta Set how much of the grid is to be plotted.

loops How many loops are to be made before stopping the simulation. The grid is redrawn after each loop.

iterations How many iterations are to be made during one loop. A high value gives less plots and thus a slightly lower run time.

min/max rho, v, P, T Determines the scaling of the palette. If you are particularly interested in resolving some aspect of the simulation, use these.

autoscale Automatically searches the grid for the highest and lowest values and updates the min/max parameters accordingly.

get total Integrates the total mass loss of the active wind over time and angle, from *phase time* to endtime taking the parameter changes during *switch time* into account.

phase time The time counter for each phase, set to zero at a new phase.

switch time If you want a smooth transition of the wind parameters between the phases. Uses a polynomial to interpolate the wind parameters at *phase time*, from zero to *switch time*. After this time, values will be constant.

end time When the program is to halt the simulation.

save prefix The name of the file that is to be saved. Will get a suffix which is the iteration count.

save frequency Tells the computer at which iterations to save a file to the disk, e.g 400 will result in files at i=400, i=800 and so forth.

load filename The name of the file you want to load.

save par If you want a file containing the parameter values used for each iteration. Only useful if you want to make a plot of the values of a short phase where you change the parameters with *switch time*

phase II When you want to use the distribution function on the velocity as well. The velocity is normalized so that the polar velocity is the same for both previous and active wind. The β of the active wind is used.

epsilon The ϵ used for smoothing.

epsilonN How many iterations to pass between each smoothing. Sometimes it may be better to do a serious smooth once every 100th iteration, instead of a little every iteration.

Runtime The only difference between this menu and **Initial**, is that you here only gain access to run time parameters. Also, the grid is not initialized after you exit, which makes it possible to enter new wind parameters, saving, or such without clearing the grid.

Movie If you find it dull staring at the screen for 15 hours as your simulation slowly progress, this is the function you need.

save filename The name of your animation.

clip freq How often a snapshot of the screen is to be taken

load filename The name of an animation you want to load.

record state Which quantity is to be recorded. 0:Rho, 1:Velocity, 2:Pressure or 3:Temperature.

record Record - on/off switch.

fullscreen If you want to show the animation for your nearsighted grandma.

play speed Does not work. Yet.

draw Choose if you want the animation played in 1D, 2D or 3D.

load Loads an animation. Remember to attach .mpig to the file name.

play Showtime!

Render To calculate a fake image of the nebula you've created, seen from somewhere far away, like earth. Handy when you want to compare your simulation to real observations. The intensity is given by the density squared, and the image is then normalized to fit the colour scale. Perhaps not the most ambitious or correct way, but serves its purpose of giving an idea of how the structure you have created look when projected on the sky.

A.3 Running a simulation

Running a simulation is pretty easy. Begin by using the *initial* screen to set the basic parameters. Before doing the real simulation, it is best to run a low resolution simulation, so set the grid size to 100×100 - 200×200. Also begin with a high value for the *super-bee* parameter, 1.8 is reasonable.

Set the parameters for the first and second phase winds. Try to use a velocity driven wind.

It is always best to run just a couple of iterations until you know all is working well, so begin by doing 5 loops of 25 iterations. Set the *phase time* to zero, the *switch time* and *end time* to what you want. Do not use any smoothing until you know it is absolutely necessary, i.e set *epsilon* and *epsilon N* to zero. Finally choose a name for the save-files and exit.

The grid is now initialized. If the scaling is wrong, go to back and click *autoscale*. All you have to do now is to press start, sit back and watch the show. You will not have any contact with the interface until either the simulation is stopped due to negative densities, the number of iterations has been made or the *end time* has been reached. If you want to change parameters without re-initializing the grid you must use the *runtime* screen.

When doing a simulation of more than two wind phases you simply go to the *runtime* screen and enter new values for the active wind. If you use the *switch time* function you must copy the values of the active wind to the row above, and it is recommended to do so any way. Also remember to save after each phase, new wind parameters often means new troubles.

A.4 File format

If you want to create your own initial conditions, or use another program to plot the grid values, it is good to know how the file data is saved. The structure is simple:

(i:integer, d:double floating point)

meshR (i)
meshTheta (i)
dtFactor (d)
gamma (d)
sbpar1 (d)
sbpar2 (d)
r1 (d) (inner radius)
r2 (d) (outer radius)
dR (d) (radial size of a grid cell)
dTheta (d) (angular size of a grid cell)
dM1 (d)
dM2 (d)
v1 (d)
v2 (d)
Q1 (d)
Q2 (d)
beta1 (d)
beta2 (d)
T1 (d)
T2 (d)

min/max (8×d)
total time (d)
total iterations (i)
phase time (d)
switch time (d)
end time (d)
cell values ({meshR+2}×{meshTheta+2}×5×d)

The cell values are ρ, ρv_r, ρv_θ, e and P. Note that they are stored as columns.